Acta Pharmaceutica Sinica B 2026;16(1):287−304

Chinese Pharmaceutical Association
Institute of Materia Medica, Chinese Academy of Medical Sciences

Acta Pharmaceutica Sinica B

www.elsevier.com/locate/apsb
www.sciencedirect.com

ORIGINAL ARTICLE

DHL-11, a novel prieurianin-type limonoid isolated from *Munronia henryi*, targeting IMPDH2 to inhibit triple-negative breast cancer

Yu Zhu[a,c,†], Zhibi Zhang[b,†], Xueqin Dai[b,†], Wenjing Liu[b], Jian Sun[d], Jialing Liu[d], Yuxin Zhao[d], Wenlong Ren[a,b], Chenglong Pan[e], Zhongmei Zhou[f,*], Ying Yan[g,*], Longlong Zhang[b,*], Ceshi Chen[b,d,*]

[a]*School of Life Science, University of Science and Technology of China, Hefei 230027, China*
[b]*Yunnan Key Laboratory of Breast Cancer Precision Medicine, Institute of Biomedical Engineering, Kunming Medical University, Kunming 650000, China*
[c]*Yunan Key Laboratory of Animal Models and Human Disease Mechanisms, Kunming Institute of Zoology, Chinese Academy of Sciences, Kunming 650201, China*
[d]*Yunan Key Laboratory of Breast Cancer Precision Medicine, Yunnan Cancer Hospital, The Third Affiliated Hospital of Kunming Medical University, Peking University Cancer Hospital, Kunming 650118, China*
[e]*Department of Pathology, Kunming Medical University First Affiliated Hospital, Kunming 650032, China*
[f]*School of Continuing Education, Kunming Medical University, Kunming 650021, China*
[g]*State Key Laboratory of Functions and Applications of Medicinal Plants & College of Pharmacy, Guizhou Provincial Engineering Technology Research Center for Chemical Drug R&D, Guizhou Medical University, Guiyang 561113, China*

Received 10 March 2025; received in revised form 4 April 2025; accepted 10 April 2025

KEY WORDS

Limonoids;
DHL-11;
TNBC;
ROS;
DNA damage;
IMPDH2;

Abstract Triple-negative breast cancer (TNBC) is the most aggressive subtype of breast cancer, characterized by the poorest prognosis, and poses a significant threat to women's health. In this study, we identified two novel prieurianin-type limonoids extracted from *Munronia henryi*, one of which, named DHL-11, exhibited antitumor activity against TNBC cells. DHL-11 suppressed cell proliferation and migration, induced G2/M cell cycle arrest and apoptosis, and effectively increased the accumulation of reactive oxygen species (ROS) and cellular DNA damage in TNBC cells. Mechanistically, we found that DHL-11 binds to the non-catalytic pocket of IMPDH2 and disrupts the interaction between IMPDH2 and

*Corresponding authors.
E-mail addresses: chenc@kmmu.edu.cn (Ceshi Chen), zhanglonglong@kmmu.edu.cn (Longlong Zhang), crystal_yanying@126.com (Ying Yan), zhouzhongmei@kmmu.edu.cn (Zhongmei Zhou).
[†]These authors made equal contributions to this work.
Peer review under the responsibility of Chinese Pharmaceutical Association and Institute of Materia Medica, Chinese Academy of Medical Sciences.

https://doi.org/10.1016/j.apsb.2025.10.031

Guanine;
FANCI

FANCI, leading to the degradation of the IMPDH2 protein. The decrease of IMPDH2 protein reduced guanine synthesis, increased ROS levels, and induced DNA damage. DHL-11 significantly inhibited the growth of breast cancer patient-derived organoids with high IMPDH2 expression. Furthermore, DHL-11 inhibited the growth and metastasis of TNBC xenografts *in vivo* with favorable biosafety profiles. Our findings highlight the potential of DHL-11 as a novel IMPDH2 degrader for the treatment of IMPDH2-positive TNBC.

1. Introduction

Breast cancer is the most common cancer among women and the leading cause of cancer-related deaths, presenting a significant threat to women's health worldwide[1]. It is a highly diverse group of malignant tumors, with different pathological features that lead to unique subtypes, each requiring specific treatments[2]. Clinically, breast cancer is classified into three main subtypes based on the expression of estrogen receptor (ER), progesterone receptor (PR), and human epidermal growth factor receptor 2 (HER2): ER-positive, HER2-positive, and triple-negative breast cancer (TNBC), which is characterized by the absence of ER, PR, and HER2 expression[3-5]. TNBC is particularly aggressive, with high mortality rates, poor prognosis, and a significant risk of recurrence and metastasis. The limited availability of targeted therapies for TNBC highlights the critical demand for the development of novel targeted treatments[4,6,7].

Reactive oxygen species (ROS) are reactive molecules derived from oxygen. ROS play a multifaceted role in cancer cells. On the one hand, cancer cells regulate the oxidative stress environment to produce specific levels of ROS, which, in turn, promote tumor cell growth and survival[8-12]. On the other hand, due to their reactive chemical properties, excessive production of ROS can damage cellular macromolecules, including DNA, lipids, and proteins. ROS-induced DNA damage leads to a variety of modification products, such as oxidatively damaged bases (*e.g.*, 8-oxo-dG), DNA single-strand breaks (SSBs), inter- and intra-strand DNA crosslinks, and DNA-protein crosslinks, ultimately resulting in necrosis and apoptosis[13,14]. In cancer cells, altered metabolic processes lead to increased production of ROS. Consequently, DNA damage induced by ROS plays a significant role in genotoxic cancer therapies[15].

Fanconi anemia (FA) is a rare inherited syndrome that increases the risk of cancer. It is caused by germline mutations in any of the 19 known FA genes (such as *FANCA* to *FANCV*). These mutations result in genomic instability, bone marrow failure, and a heightened risk of developing cancer, particularly acute myeloid leukemia[16]. The FA pathway repairs DNA interstrand crosslinks (ICLs) through coordinated mechanisms, including translesion synthesis (TLS) and homologous recombination (HR). The monoubiquitination of the FANCD2/FANCI complex serves as a crucial regulatory step in activating DNA repair[17-19]. Overexpression of Fanconi anemia complementation group I (FANCI) is associated with poor prognosis in liver hepatocellular carcinoma and skin cutaneous melanoma[20,21]. In contrast, inhibiting FANCI can reverse chemoresistance and improve the effectiveness of treatments when combined with PARP inhibitors, such as talazoparib, or CDK4/6 inhibitors like palbociclib[22]. Targeting FANCI reprograms DNA repair deficiencies, thereby providing new therapeutic strategies to overcome drug resistance and expand the clinical applications of current anticancer therapies.

Purine nucleotides play a crucial role in various cellular processes, including DNA and RNA biosynthesis, DNA repair, signal transduction, and metabolic pathways. Human inosine monophosphate dehydrogenase (IMPDH) catalyzes the conversion of inosine 5′-monophosphate (IMP) to xanthine 5′-monophosphate (XMP), which is a key step in guanine nucleotide production. As the rate-limiting enzyme in the *de novo* synthesis of guanine, IMPDH is essential for nucleotide homeostasis. There are two isoforms of human IMPDH: IMPDH1 and IMPDH2, which share 84% sequence homology[23]. IMPDH1 is predominantly expressed in the immune system, particularly in the spleen and peripheral blood mononuclear cells. In contrast, IMPDH2 is an inducible enzyme that is significantly upregulated in tumor tissues and in rapidly proliferating cells[24]. IMPDH2 is implicated in various types of malignant tumors, including colorectal, prostate, kidney, and bladder cancers. Moreover, it can activate multiple signaling pathways, such as the PI3K−Akt pathway, which promotes tumor growth and progression[25-27]. Previous studies have demonstrated that the knockdown of IMPDH2 leads to the accumulation of ROS and induces ferroptosis in hepatocellular carcinoma cells. In addition, the deletion of both IMPDH1 and IMPDH2 results in DNA damage and increases the sensitivity of glioblastoma cells to temozolomide (TMZ)[28]. Inhibition of IMPDH2 activity similarly enhances TMZ-induced DNA damage in glioblastoma[29]. FANCI is a crucial protein involved in ribosome biogenesis and DNA repair; it binds to IMPDH2, stabilizing the enzyme and promoting lung cancer progression[30]. In breast cancer, IMPDH2 activates the NF-κB signaling pathway to upregulate inflammatory mediators[31,32].

Several IMPDH2 inhibitors have been identified to date[33]. Mycophenolic acid (MPA) is an FDA-approved dual inhibitor of IMPDH1 and IMPDH2, currently used to treat inflammation[34]. MPA can inhibit tumor growth and metastasis in colorectal and lung cancers[35,36]. In addition to MPA, several IMPDH2 inhibitors derived from natural products have been reported. Pan et al.[37] identified myricetin, a compound found in berries, as a dual inhibitor of IMPDH1 and IMPDH2. Furthermore, berberrubine and shikonin are specific inhibitors of IMPDH2, demonstrating antitumor activity in colorectal and breast cancers[38,39]. Liao et al.[31] showed that sappanone A covalently binds to Cys140 of IMPDH2, thereby inactivating the enzyme. However, because of the essential role of IMPDH1 in normal physiological processes, non-selective inhibitors of IMPDH1 and IMPDH2 have been linked to severe gastrointestinal side effects[40]. Therefore, discovering effective and selective IMPDH2 inhibitors for cancer treatment is critical.

Limonoids are natural tetranortriterpenoids characterized by a distinctive 17β-furan ring system, primarily found in the Meliaceae and Rutaceae families. They are structurally classified into

three main types: ring-intact, ring-seco, and rearranged, which are widely accepted as classification standards[41-43]. A broad range of limonoids exhibit various biological activities, including anti-tumor, anti-inflammatory, antibacterial, anti-HIV, metabolic regulatory, insecticidal, and antiviral properties[44-47]. Among these compounds, nimbolide, nomilin, and gedunin are particularly recognized for their antitumor activity[48,49]. Due to their unique structural frameworks and significant biological effects, limonoids remain a popular subject of research. However, despite their potent antitumor effects in breast, pancreatic, liver, and colon cancers, the underlying mechanisms of action are still unclear, which limits their clinical applications[48,50].

In this study, we identified two limonoids extracted from *Munronia henryi*, among which DHL-11 demonstrated strong antitumor activity in TNBC. Mechanistic characterization revealed that DHL-11 effectively inhibits the proliferation and migration of TNBC cells by binding to the non-catalytic pocket of the IMPDH2 protein, leading to its degradation. Notably, DHL-11 and MPA bind to distinct sites on IMPDH2 (Fig. 1).

2. Materials and methods

2.1. Cell culture and treatment

The cell lines used in this study were sourced from the American Type Culture Collection (ATCC, Manassas, VA, USA) and authenticated through short tandem repeat (STR) analysis. The TNBC cell line MDA-MB-231 was cultured in DMEM/F12 (Gibco, USA) supplemented with 10% fetal bovine serum (FBS), while HCC1806 cells were cultured in RPMI1640 (Gibco, USA) with 5% FBS. All cell lines were maintained in a 5% CO_2 incubator at 37 °C. Detailed information on the culture conditions for the other cell lines used in this study can be found in Supporting Information Table S1.

2.2. Antibodies and reagents

The following antibodies were used in this study: CDC2 (77055S, 1:1000), Cyclin B1 (sc-245, 1:1000), p-27 (3686S, 1:1000), Bcl-2 (3498, 1:1000), Caspase-8 (9746, 1:1000), Caspase-9 (9502, 1:1000) from Cell Signaling Technology (Boston, USA); CDC25 (A12234, 1:1000) from Proteintech (Chicago, IL, USA) GAPDH (SC-32233, 1:1000) and FANCI (A-7: sc-271316, 1:1000) from Santa Cruz Biotechnology (CA USA); Vinculin (V9131, 1:1000) from Sigma−Aldrich (St. Louis, MO, USA); IMPDH2 (R26909, 1:1000) from Zenbio (Chengdu, China); γH2AX (AP0687) from ABclonal; and Ki-67 (MAB-0672) from MXB Biotechnologies.

2.3. Compound isolation

The air-dried and powdered plant material (9.5 kg) was extracted with methanol (MeOH) (3 × 40 L) under reflux for three consecutive periods (4, 3, and 3 h). The combined MeOH extracts were concentrated under vacuum to yield a crude residue (1.32 kg), which was then suspended in water and partitioned with ethyl acetate (EtOAc). The EtOAc fraction (193 g) was loaded onto a silica gel column and eluted with a gradient of petroleum ether (PE)−EtOAc (50:1 to 1:1, *v*/*v*) followed by dichloromethane (CH_2Cl_2)−methanol (CH_3OH) (15:1 to 1:1, *v*/*v*), resulting in seven fractions (Fr.1−Fr.7). Fraction 6 (21.4 g) was further separated using an MCI-gel column, eluted with a MeOH−H_2O gradient (3:7 to 10:0, *v*/*v*), yielding six fractions (Fr. 6A−Fr. 6F). Fraction 6C (3.6 g) was chromatographed on a C18 silica gel column, eluted with a MeOH−H_2O gradient (5:5, 6:4, 7:3, and 8:2, *v*/*v*), affording five subfractions (Fr. 6Ca−Fr. 6Ce). Fraction 6Cd (1.5 g) was further purified using silica gel chromatography ($CHCl_3$−MeOH, 25:1, *v*/*v*) and Sephadex LH-20 (MeOH), yielding DHL-10 (32.5 mg) and Fraction 6Cd1. Fraction 6Cd1

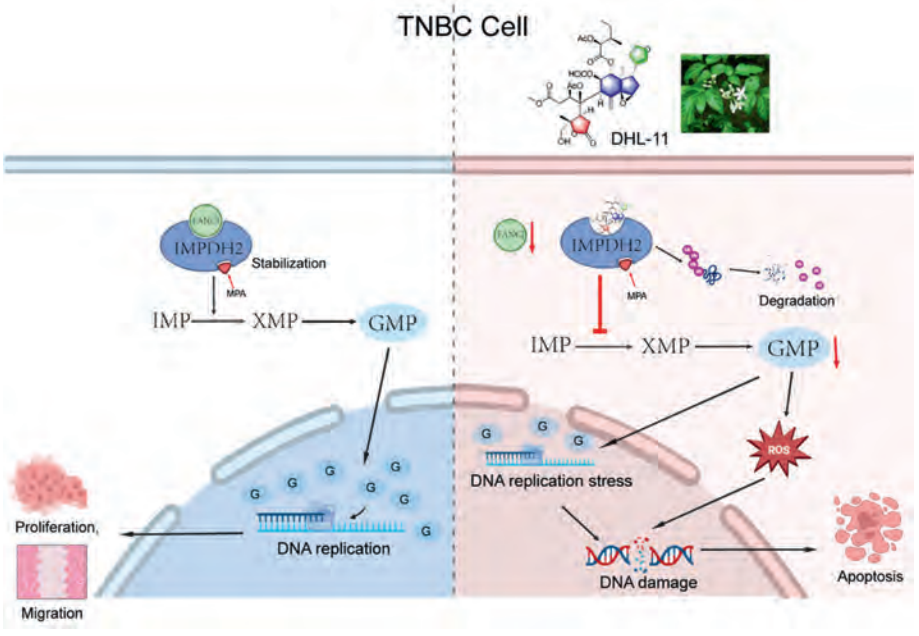

Figure 1 DHL-11 competes with FANCI to bind IMPDH2, thereby reducing the stability and promoting the degradation of IMPDH2, this reduction in IMPDH2 levels leads to a decrease in intracellular GMP synthesis, which in turn induces ROS accumulation. The increased ROS accumulation results in DNA damage and DNA replication stress in TNBC cells, ultimately leading to apoptosis of TNBC cells.

(528 mg) was subjected to semipreparative HPLC (MeOH−H2O, 65:35, *v/v*) to obtain DHL-11 (346 mg, t_R = 25 min)[51].

2.4. RNAi and transfection

siRNA transfection was performed using Opti-MEM (Gibco, USA) and Lipofectamine 2000 (Invitrogen) according to the manufacturer's instructions. The siRNAs, synthesized by Qingke Bio, were transfected at a final concentration of 10 nmol/L. The target sequences for si*IMPDH2* were: 1#: GGUAUGGG UUCUCUCGAUG, 2#: AAGGGUCAAUCCACAAAUU.

si*TRAF3IP2* were 1#: sense (5′−3′): GAUAAGACCGUGAUG AUAATT, antisense (5′−3′): UUAUCAUCACGGUCUUAUCTT; 2#: sense (5′−3′): GCUCCAAAUAUAAGGAACATT, antisense (5′−3′): UGUUCCUUAUAUUUGGAGCTT;

si*PLK1* were 1#: AGAUUGUGCCUAAGUCUCU, 2#: AGAC UCAGGCGGUAUGUGC.

si*FANCI* were 1#: CUGGCUAAUCACCAAGCUUAA, 2#: UUGAAUUUACUUAGCAGUCAA.

2.5. Plasmids, transfection, and lentivirus

The *IMPDH2* and *FANCI* genes were constructed in the pCDH vector. Lentiviruses were packaged in HEK293T cells using 1 μg of plasmid and 4 μL of PEI (polyethylenimine, Plybiosciences). The packaging plasmids used included psPAX2 (3 μg), pMD2.G (1 μg), in combination with the pCDH-IMPDH2-3′Flag (4 μg). The lentiviral supernatant was harvested 48 h post-transfection. The virus was then used to infect target cells, and the cells were selected with puromycin (1 μg/mL) 48 h later.

2.6. ROS detection

Intracellular ROS levels were measured using the Reactive Oxygen Species Assay Kit (S0033, Beyotime). Briefly, cells were processed and then incubated in serum-free medium containing the fluorescent probe DCFH-DA (1:1000 dilution) for 30 min. After digestion, the cells were resuspended in PBS. The fluorescence intensity was detected by flow cytometry and analyzed using FlowJo software.

2.7. Patient-derived breast cancer organoids and drug treatment

Primary breast cancer specimens were obtained from patients who underwent surgical excision or puncture of breast cancer at Yunnan Cancer Hospital. This study was approved by the Clinical Research Ethics Committee of Yunnan Cancer Hospital (KYCS2023-078). The primary breast cancer tissue samples were stored in serum-free DMEM/F12 medium with 1% penicillin/streptomycin solution (Solarbio) and transported to the laboratory in a low-temperature incubator. The breast cancer tissue was washed three times with PBS and then minced into small pieces in a 1.5 mL centrifuge tube. The small tissue pieces were dissociated using Tumor Tissue Digestion (Biogenous) and incubated at 37 °C for 1−2 h. Digestion was completed by adding DMEM/F12 with 10% FBS until the large tissue pieces were reduced and most cells were in suspension. The suspension cells were filtered through a 100 μm cell strainer and subsequently centrifuged at 1000 rpm for 5 min. The cells were incubated in Erythrocytes Lysate (Biosharp) for 2 min at 4 °C to lyse residual red blood cells. The cells were then mixed with growth factor-reduced Matrigel (Biogenous) and seeded into 24-well plates. Warm breast cancer organoid medium was added after the Matrigel solidified within 20 min. DHL-11 was dissolved in DMSO and stored at −80 °C. Breast cancer organoids were digested into small clusters and filtered through a 40 μm cell strainer to eliminate larger cell clusters. The organoids were seeded into 96-well plates at a density of approximately 3000 cells in 3 μL of Matrigel. After 2 days of plating, the organoids were treated with seven concentrations of DHL-11 ranging from 0, 1, 6, to 10 μmol/L. The viability of the organoids was analyzed using the Organoids Viability ATP Assay Kit (Biogenous) after 3 days of drug incubation.

2.8. Molecular docking and molecular dynamics simulation

The crystal structure of human IMPDH2 (PDB ID: 1NF7) was downloaded from the Protein Data Bank (https://www.pdbus.org/). Crystallographic water molecules and heteroatoms were removed, and the atomic coordinates of IMPDH2 were saved. The 3D structure of DHL-11 was generated using Avogadro 1.2.0, and the structure of MPA was obtained from PubChem (CID: 446541). AutoDock Vina 1.2.0 (10.1002/jcc.21334) was used to dock DHL-11 and MPA separately to the catalytic domain of IMPDH2 to predict their binding modes. Molecular dynamics simulations were performed for 200 ns using GROMACS 5.1.4 (https://www.softxjournal.com/article/S2352-7110(15)00005-9/fulltext) with the AMBER99SB-ILDN force field (10.1002/prot.22711). Force field parameters for DHL-11 and MPA were generated using the General Amber Force Field (GAFF) *via* AmberTools20. Root mean square deviation (RMSD) values were calculated from the molecular dynamics simulation trajectories, and representative conformations were extracted for binding free energy calculations using gmx_MMPBSA (10.1021/acs.jctc.1c00645) to assess the binding stability and affinity of the DHL-11 and MPA complexes with IMPDH2. The binding mode between IMPDH2 and FANCI was predicted using AlphaFold 3 (10.1038/s41586-024-07487-w), and residue interaction information between the two proteins was visualized using PDBsum (10.1002/pro.3289).

2.9. RNA-seq analysis

The HCC1806 cell line was seeded in 6-well plates and treated with DMSO or DHL-11 (1 μmol/L) for 24 h. RNA samples were extracted using Trizol and subsequently sent to Lianchuan Biologicals for high-throughput sequencing. Fastp software was used to remove reads containing adaptor contamination, low-quality bases, and undetermined bases with default parameters. HISAT2 was then used to map the reads to the reference genome of *Homo sapiens* GRCh38. All transcriptomes from the samples were merged to reconstruct a comprehensive transcriptome using gffcompare. StringTie was employed to calculate the expression levels of mRNAs by determining FPKM values. Differentially expressed mRNAs were identified with a fold change greater than 2 or less than 0.5, using a parametric F-test for comparing nested linear models (P-value <0.05) *via* the R package edger. Finally, the genes were analyzed for GO and KEGG enrichment using DAVID software.

2.10. Target capture technology

MS-SPRi was utilized to elucidate the protein target of DHL-11 in HCC1806 cells. Briefly, total proteins from HCC1806 cells were extracted by incubating the cells in lysis buffer. The extracted proteins were then passed through a nanosensor chip to identify

those immobilized by DHL-11. Proteins or peptides captured by DHL-11 were digested *in situ* with trypsin and subsequently identified using HPLC−MS/MS. The MS data were analyzed using MaxQuant software (COX LAB, version 1.3.0.5). The captured peptides and proteins were further analyzed using Proteome Discoverer (Thermo Fisher Scientific, version 1.7) by searching the UniProtKB/Swiss-Prot database[52].

2.11. Surface plasmon resonance (SPR)

Surface Plasmon Resonance (SPR) analysis was conducted to determine the dissociation constant (K_D) values using a Biacore S200 system. A CM5 sensor chip was employed to capture the IMPDH2 protein, with PBST (0.05% Tween 20 in PBS) containing 5% DMSO as the running buffer. The recombinant IMPDH2 protein was immobilized on the CM5 chip at pH 4.5. To evaluate binding affinity and determine the K_D value, each compound was diluted to concentrations of 64, 32, 16, 8, 4, and 2 μmol/L. The data were analyzed using Biacore S200 analysis software. Competition assays following the A−B−A injection model were performed as previously described[53]. Solution A consisted of 8 μmol/L MPA (MCE, China, HY-B0421), and Solution B comprised 8, 16, or 32 μmol/L DHL-11 alone or in combination with 8 μmol/L MPA. The blocking efficacy was assessed by comparing the response units with and without incubation with Solution A.

2.12. Cellular thermal shift assays

Cells were cultured in 10 cm dishes and treated with either DMSO or DHL-11 (4 μmol/L) for 4 h. Subsequently, the cells were digested and resuspended in PBS. They were then divided into different groups and exposed to various temperature gradients for 3 min. Following this, the samples were lysed and subjected to Western blotting analysis.

2.13. Drug affinity responsive target stability (DARTS)

The Drug Affinity Responsive Target Stability (DARTS) assay is based on the principle that small molecules become resistant to protease degradation when they bind to target proteins. The specific experimental methods have been described previously[54]. Briefly, cells were lysed for protein quantification, and either DMSO or varying concentrations of DHL-11 were added for 30 min at room temperature. Subsequently, an appropriate proportion of proteinase K was added for 5 min at room temperature, followed by Western blot analysis.

2.14. HPLC−MS analysis for intracellular guanosine

Cells were inoculated in 10 cm dishes and treated with either DHL-11 or DMSO for 24 h. The cells were then digested and washed with PBS. The precipitate was centrifuged, and the cells were resuspended in 80% methanol (80% methanol and 20% water). The resuspended cells were sonicated and lysed on ice for 30 min. The subsequent cell lysates were analyzed by liquid chromatography coupled with mass spectrometry, as described in previous studies[55].

2.15. RNA extraction and reverse transcription-quantitative PCR (RT-qPCR)

Total mRNA was extracted using Trizol reagent (Sigma). Subsequently, cDNA synthesis was performed with the HiScript II Q RT SuperMix for qPCR (+gDNA wiper) Kit according to the manufacturer's instructions. RT-qPCR was conducted using specific primers and SYBR qPCR Master Mix (Roche, Basel, Switzerland) on a QuantStudio 3 instrument (Applied Biosystems). Relative expression levels were determined using the $2^{-\Delta\Delta Ct}$ method, with 18S rRNA serving as the reference gene for normalization. The following primer sequences were used for the qPCR:

IMPDH2 forward, 5′-CCGACTACCTGATTAGTGGGG-3′ and reverse, 5′-GTCTCCGCAGTTGAAGAGC-3′;

18S forward, 5′-CCTGAGAAACGGCTACCACATC-3′ and reverse, 5′-GCCTCGAAAGAGTCCTGTATTG-3′.

2.16. Immunohistochemical (IHC) staining

IHC staining was performed as previously described[56]. An anti-Ki67 antibody (Fuzhou Maixin Biotech, China) was used to analyze cell proliferation.

2.17. Animal experiments

Female nude mice were obtained from SJA Lab Animal Co., Ltd. (Changsha, China) and injected with HCC1806 cells (1×10^6 cells/spot) *via* bilateral orthotopic fat pad injection. When the tumors reached a size of 50 mm^3, the mice were randomly divided into control and experimental groups (DHL-11, 3 mg/kg) and administered the treatment by gavage every other day until the 13th day. Tumor size was measured every 2 days using a vernier callipers. At the end of the experiment, tumors were harvested for analysis. *In vivo* toxicity assays of the compounds were also performed. After anesthetizing the mice, blood was collected *via* retroorbital bleeding and centrifuged at 4000 rpm for 20 min. The blood was then tested using AST, ALT, and CRE test kits (Nanjing Jiancheng Bioengineering Institute) according to the manufacturer's instructions. Stably IMPDH2-overexpressing HCC1806 or control HCC1806 cells were injected into the bilateral mammary fat pads of female BALB/c nude mice (1×10^6 cells/spot). When tumor volumes reached 50 mm^3, mice were randomly allocated to receive either DMSO (vehicle control) or DHL-11 (3 mg/kg) *via* oral gavage. Treatment was administered for three consecutive days followed by one day of rest until the 9th day, after which tumors were harvested. Mouse body weight and tumor volume were measured twice weekly. For the metastasis assay, 5-week-old nude mice were intravenously injected with 4T1 cells (1×10^6 cells/mouse) *via* the tail vein. From the next day, mice were treated with DMSO or DHL-11 (3 mg/kg) by oral gavage, following the same dosing schedule (three days on, one day off until Day 9). Lung tissues were collected after treatment for further analysis. All mice were kept in specific pathogen-free (SPF) conditions at the Animal Resource Centre of the Kunming Institute of Zoology, Chinese Academy of Sciences. All animal experiments were conducted in accordance with the guidelines and were approved by the Animal Care and Use Committee of the Kunming Institute of Zoology, Chinese Academy of Sciences (IACUC-RE-2024-11-001).

2.18. Statistical analysis

Statistical analyses were conducted *via* Prism v.8.0.2 (GraphPad). The error bars indicate the mean ± standard error of the mean (SEM). Two-way ANOVA or two-tailed Student's *t* test was employed to assess statistical significance. In the results, $P < 0.05$ was considered to be significant.

3. Result

3.1. DHL-11 effectively inhibits TNBC cell proliferation

We isolated two limonoids from *Munronia henryi*, both of which possess a 4,4,8-trimethyl-17-furan steroid skeleton. After forming this basic limonoid structure, various oxidations and rearrangements occurred, resulting in the production of prieurianin-type limonoid analogues, specifically DHL-10 and DHL-11 (Fig. 2A and Supporting Information Table S2). DHL-11 demonstrates significant inhibitory effects on the proliferation of ER+, HER2+, and TNBC cell lines, with IC_{50} values in TNBC cell lines lower than 1 μmol/L (Fig. 2B−D). This efficacy is comparable to that of epirubicin and lower than those of doxorubicin, palbociclib, and cisplatin (Supporting Information Fig. S1A and S1B). In contrast, DHL-10 did not show any cytotoxic effects despite its structural

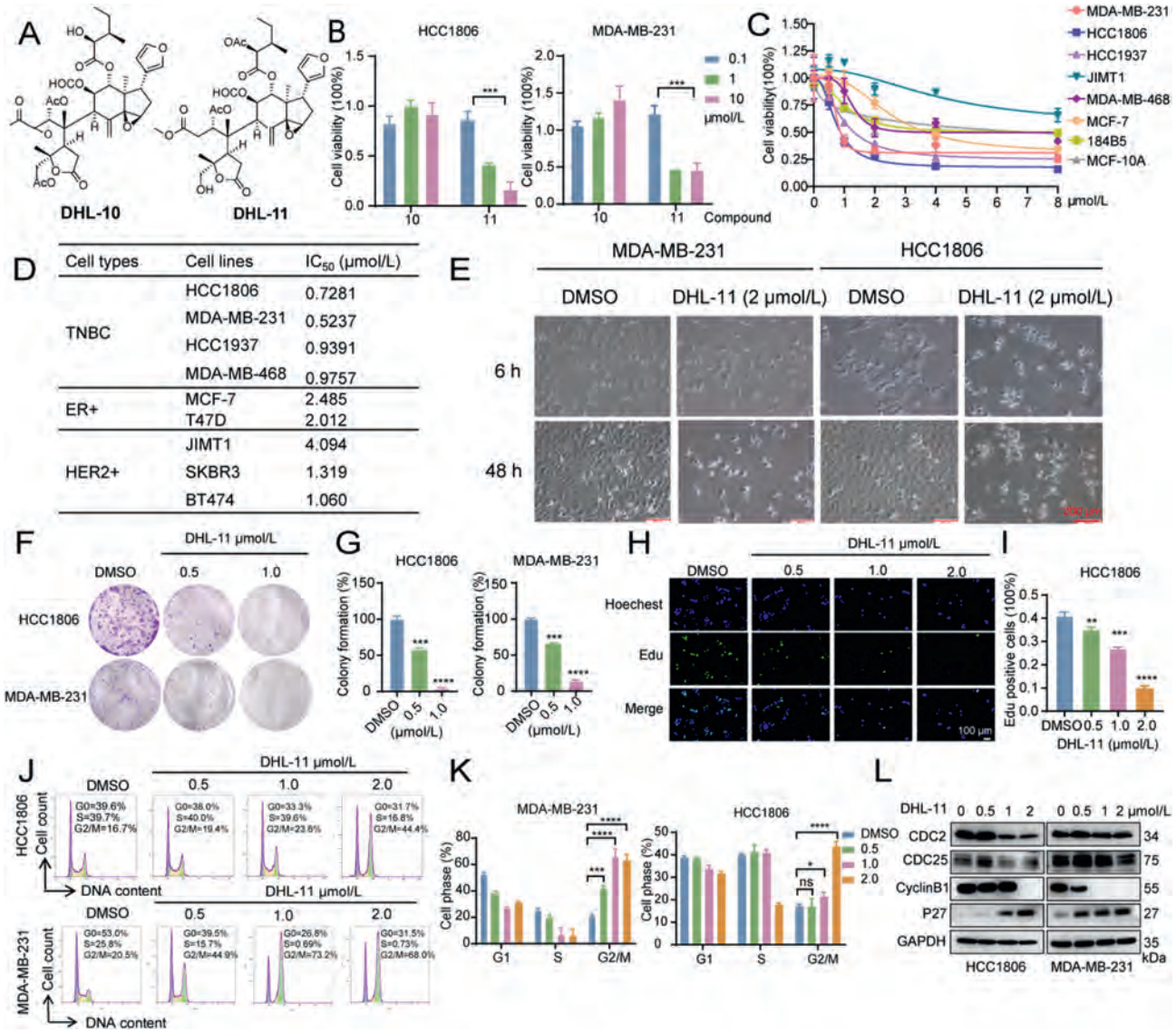

Figure 2 DHL-11 effectively inhibits TNBC cell proliferation and induces G2/M arrest. (A) Chemical structures of two natural products obtained from the extraction of *Munronia Henryi*. (B) SRB assays were applied to detect the cell viability after treatment with two natural products in MDA-MB-231 and HCC1806 cell lines. Data are presented as mean ± SD ($n = 5$). (C, D) IC_{50} of DHL-11 in the breast cancer cell lines. Data are presented as mean ± SD ($n = 5$). (E) Microscopic observation of cell morphology changes of MDA-MB-231 and HCC1806 after treatment with DHL-11. Scale bar: 200 μm. (F) The representative images of colonies after treatment with DHL-11 for 12−14 days in HCC1806 and MDA-MB-231 cells. (G) Quantification of the number of colonies after treatment with DHL-11. Data are presented as mean ± SD ($n = 3$). (H) Edu incorporation for microscopy analysis of cellular DNA synthesis after treatment with DHL-11 in HCC1806 cells. (I) The quantification of the proportion of EdU-positive cells. Data are presented as mean ± SD ($n = 3$). (J) MDA-MB-231 and HCC1806 cells were treated with DHL-11 for 48 h and then processed for cell cycle analysis by flow cytometry using PI staining. (K) Quantification of the proportion of each phase of the cell cycle. Data are presented as mean ± SD ($n = 3$). (L) DHL-11 regulated cell cycle-related proteins. Western blot was used to detect the expression levels of CDC2, CDC25, cyclin B1 and p27 in MDA-MB-231 and HCC1806 cells after treatment with DHL-11 at different concentrations for 48 h. GAPDH was used as the internal control. Data are representative of at least three independent experiments. $^{*}P < 0.05$, $^{**}P < 0.01$, $^{***}P < 0.001$ and $^{****}P < 0.0001$; ns, no statistically significant difference.

similarity to DHL-11. The concentration gradient and time gradient treatment of DHL-11 significantly induced the shrinkage and apoptosis of TNBC cells (Fig. 2E). DHL-11 consistently decreased DNA synthesis in TNBC cells and inhibited the formation of TNBC cell clones in a dose-dependent manner (Fig. 2F−I and Fig. S1C and S1D). Cell cycle analysis revealed that DHL-11 induces cell cycle arrest at the G2/M transition in HCC1806 and MDA-MB-231 cells (Fig. 2J and K). Furthermore, DHL-11 significantly reduced the expression levels of key cell cycle-related proteins, including CDC2, CDC25, and Cyclin B1, while increasing the expression of p27 (Fig. 2L). These findings support the conclusion that DHL-11 inhibits the proliferation of TNBC cells. However, DHL-11 did not significantly induce cell cycle arrest in HER2+ (JIMT1) and ER+ (MCF-7) breast cancer cells at a concentration of 2 μmol/L (Supporting Information Fig. S1E−S1G). This suggests that DHL-11 exhibits stronger inhibitory effects on TNBC cells compared to HER2+ and ER + subtypes.

3.2. *DHL-11 inhibits TNBC cell migration and survival*

We conducted a wound healing assay that showed DHL-11 inhibited the migration of TNBC cells in a dose-dependent manner (Fig. 3A and B). Similarly, the transwell assay demonstrated a concentration-dependent reduction in TNBC cell migration induced by DHL-11 (Fig. 3C and D, Supporting Information Fig. S2A). Additionally, we used matrigel-preincubated transwell filters to assess cell invasion, and the results indicated that DHL-11 effectively inhibited the invasion of

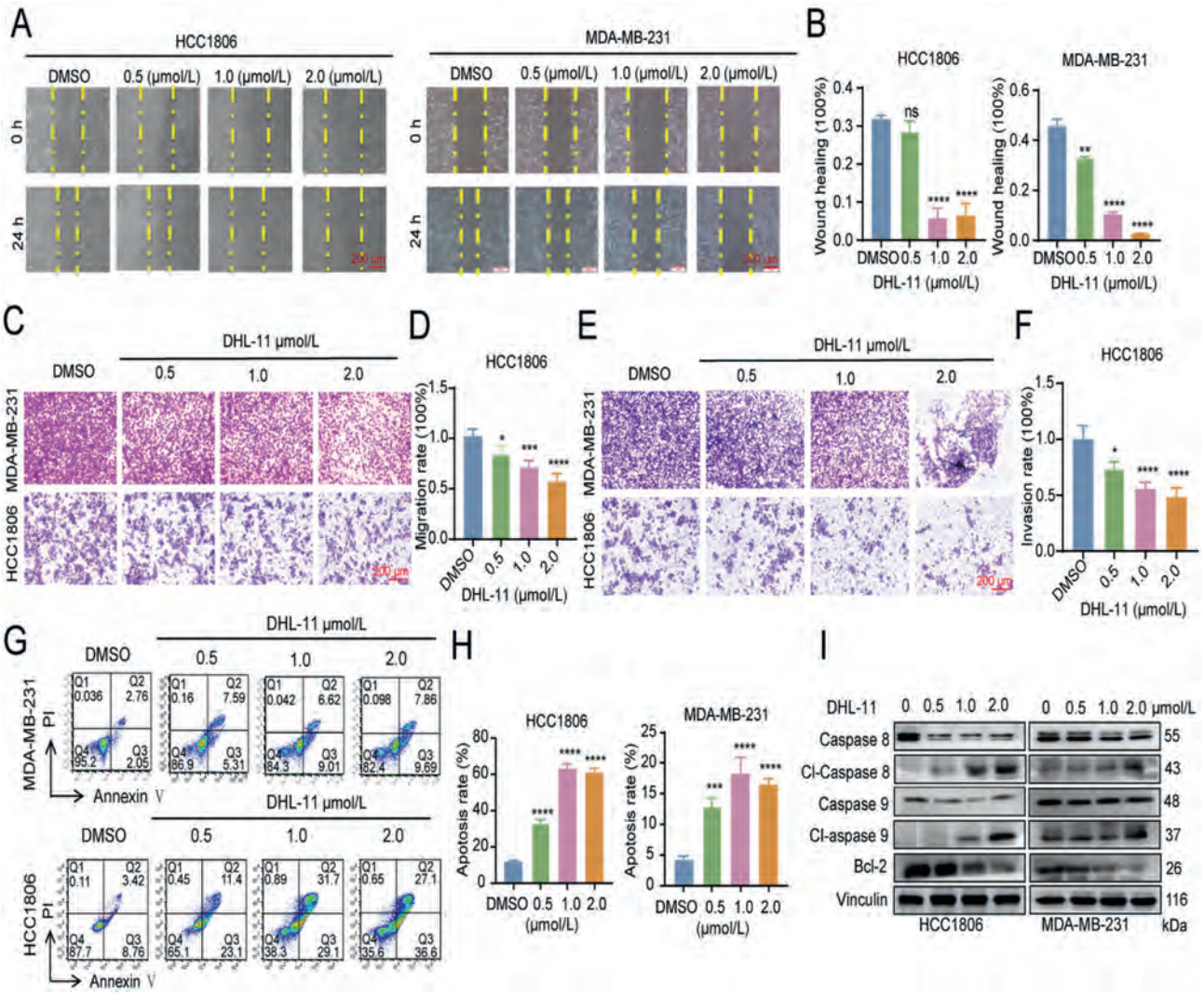

Figure 3 DHL-11 inhibits TNBC cell migration and survival. (A, B) Wound healing assays were performed to evaluate cell migration, and the crack width of the scratches was quantified after treatment with DHL-11. Scale bar: 200 μm. (C, D) Transwell assay was performed to evaluate cell migration, and the migrated cell number was quantified after treatment with DHL-11. Scale bar: 200 μm. (E, F) Transwell assay with precoated Matrigel was performed to evaluate cell invasion, and the invaded cell number was quantified after treatment with DHL-11. Scale bar: 200 μm. (G) MDA-MB-231 and HCC1806 cells were treated with DHL-11, followed by apoptosis analysis after Annexin V/PI staining with flow cytometry. (H) Quantification of the proportion of Annexin V/PI -positive cells. (I) HCC1806 and MDA-MB-231 cells were treated with the different concentrations of DHL-11 for 48 h, Western blotting was subsequently applied to detect the protein levels of Caspase 8, Caspase 9, Cl-Caspase 8, Cl-Caspase 9, Bcl2. Data are presented as mean ± SD ($n = 3$). Vinculin was used as the internal control. Data are representative of at least three independent experiments. *$P < 0.05$, **$P < 0.01$ and ***$P < 0.001$ and ****$P < 0.0001$; ns, no statistically significant difference.

MDA-MB-231 and HCC1806 cells (Fig. 3E and F, Fig. S2A). To determine if the observed inhibition of migration was due to decreased proliferation, we evaluated the impact of DHL-11 on cell viability during the first 24 h of treatment. The results showed that DHL-11 did not significantly affect cell viability within this timeframe (Fig. S2B). Thus, DHL-11 inhibits cell migration independently of its effects on proliferation.

We further investigated the role of DHL-11 in inducing apoptosis. The compound induced apoptosis in HCC1806 and MDA-MB-231 cells in a dose-dependent manner (Fig. 3G and H). Notably, DHL-11 increased the expression levels of cleaved caspase 8 and cleaved caspase 9 while inhibiting Bcl-2 expression. These findings suggest that DHL-11 may induce apoptosis through both extracellular receptor-dependent and mitochondrial pathways (Fig. 3I). Additionally, at concentrations of 0.5−2 μmol/L, DHL-11 induced minimal apoptosis in JIMT1 cells and did not induce apoptosis in MCF7 cells, with no changes in the levels of apoptotic proteins (Fig. S2C−S2E). These results reinforce the selective efficacy of DHL-11 against TNBC cells.

3.3. DHL-11 induces DNA damage by increasing the ROS levels in TNBC cells

To further explore the functional mechanism of DHL-11 in TNBC cells, we conducted RNA sequencing (RNA-Seq) to analyze differentially expressed genes (DEGs). The top 20 functionally enriched pathways were illustrated in a bubble chart based on KEGG analysis. Notably, we discovered that DHL-11 significantly regulated pathways associated with "DNA replication", "mismatch repair", "base excision repair", and the "cell cycle", all of which are involved in nucleotide metabolic processes (Fig. 4A). Subsequently, we investigated whether DHL-11 induces DNA damage and found that it markedly increased γH2AX protein levels in both MDA-MB-231 and HCC1806 cells in a dose-dependent manner (Fig. 4B−D, Fig. S2F).

ROS are significant inducers of DNA damage. Therefore, we investigated whether DHL-11 leads to the accumulation of ROS in TNBC cells. Utilizing flow cytometry, we assessed ROS levels in MDA-MB-231 and HCC-1806 cells and found that treatment with DHL-11 (0.5−2 μmol/L) significantly increased ROS levels (Fig. 4E and F). Correspondingly, the ROS inhibitor *N*-acetyl-L-cysteine (NAC) reduced both the accumulation of ROS and the levels of γH2AX protein induced by DHL-11 (Fig. 4G−I, Fig. S2G). Additionally, NAC partially reversed the inhibitory effects of DHL-11 in TNBC cells (Fig. 4J).

3.4. IMPDH2 is the target of DHL-11

To investigate the target of DHL-11, we used target capture technology based on surface plasmon resonance (SPR)[52]. The specific binding proteins were identified using high-performance liquid chromatography (HPLC) coupled with mass spectrometry (MS). The captured proteins were analyzed and presented through an MS score heatmap and a relative quantity heatmap (Supporting Information Fig. S3A and S3B). Given that DHL-11 regulates nucleotide metabolism, cell division, and the TNFA and NF-κB signaling pathways (Fig. 4A), we selected three candidate target proteins for further study: TRAF3-interacting protein 2 (*TRAF3IP2*), inosine monophosphate dehydrogenase 2 (*IMPDH2*), and polo-like kinase 1 (*PLK1*). While knockdown of *TRAF3IP2* and *PLK1* did not render TNBC cells less sensitive to DHL-11, knockdown of *IMPDH2* resulted in resistance to DHL-11 (Supporting Information Fig. S4A).

IMPDH2 catalyzes the oxidation of IMP to XMP and serves as the rate-limiting enzyme in the *de novo* synthesis of guanosine nucleotides. To determine whether IMPDH2 directly interacts with DHL-11, we conducted SPR, drug affinity responsive target stability (DARTS), cellular thermal shift assay (CETSA), and molecular docking analyses. Our SPR assays demonstrated that DHL-11 exhibited a high binding affinity for IMPDH2 in a dose-dependent manner (Fig. 5A, Fig. S4B). Molecular docking results indicated that DHL-11 binds to the non-catalytic structural domain of IMPDH2 through van der Waals forces, carbon−hydrogen bonds, π interactions, and alkyl interactions, with a binding free energy of −6.7 kcal/mol and inhibition constants of 12.33 μmol/L (Fig. 5B and C, Fig. S4C). To evaluate the stability of this binding mode, we performed a 200 ns molecular dynamics (MD) simulation and assessed the binding stability by calculating the root mean square deviation (RMSD) values of the protein Cα atoms and the inhibitor heavy atoms. Our findings revealed that, despite some fluctuations, the RMSD values consistently ranged between 0.3 and 1.0 nm, suggesting that the IMPDH2/DHL-11 complex remains stable under simulated physiological conditions (Fig. 5D). Both DARTS and CETSA assays demonstrated that DHL-11 protects IMPDH2 from proteolytic degradation and thermal instability (Fig. 5E−G), indicating that IMPDH2 is a direct binding target of DHL-11 in TNBC cells.

IMPDH2 is the rate-limiting enzyme in guanine synthesis. We utilized liquid chromatography−tandem mass spectrometry (LC−MS/MS) to analyze intracellular guanine levels in MDA-MB-231 and HCC1806 cells. Our findings indicate that DHL-11 significantly reduced the intracellular guanine content (Fig. 5H and I, Fig. S4D and S4E). The exogenous supplementation of guanine effectively inhibited the antitumor activity induced by DHL-11, as well as the increases in ROS and γH2AX levels (Fig. 5J−M, Fig. S4F). Subsequently, we established stable HCC1806 and MDA-MB-231 cell lines that overexpress IMPDH2, revealing that IMPDH2 promotes cell proliferation in TNBC cells and that overexpression of IMPDH2 rescues the growth inhibition induced by DHL-11 (Fig. 5N, Fig. S4G−S4I). Interestingly, DHL-11 markedly reduced the protein levels of both exogenous and endogenous IMPDH2, and overexpression of IMPDH2 suppressed the increase in γH2AX levels caused by DHL-11 (Fig. 5O and P). Furthermore, treatment with DHL-11 following IMPDH2 knockdown synergistically inhibited the expression levels of both IMPDH2 and γH2AX (Fig. S4J).

3.5. Unlike MPA, DHL-11 degrades IMPDH2 protein by disrupting the interaction between IMPDH2 and FANCI

MPA, an FDA-approved non-selective inhibitor of IMPDH2, binds to the catalytic pocket of IMPDH and inhibits its enzymatic activity[57]. SPR assays, molecular docking analyses, and molecular dynamics simulations confirmed that MPA binds stably to IMPDH2, although it exhibits a lower binding affinity compared to DHL-11 (Fig. 6A−E). To further investigate the structure of IMPDH2 bound to DHL-11, we conducted a competitive binding assay using the Biacore T200 to determine whether MPA influences the interaction between DHL-11 and IMPDH2. The results demonstrated that MPA enhanced the interaction between DHL-11 and IMPDH2, indicating that DHL-11 and MPA bind non-competitively to different sites on IMPDH2 (Fig. 6F).

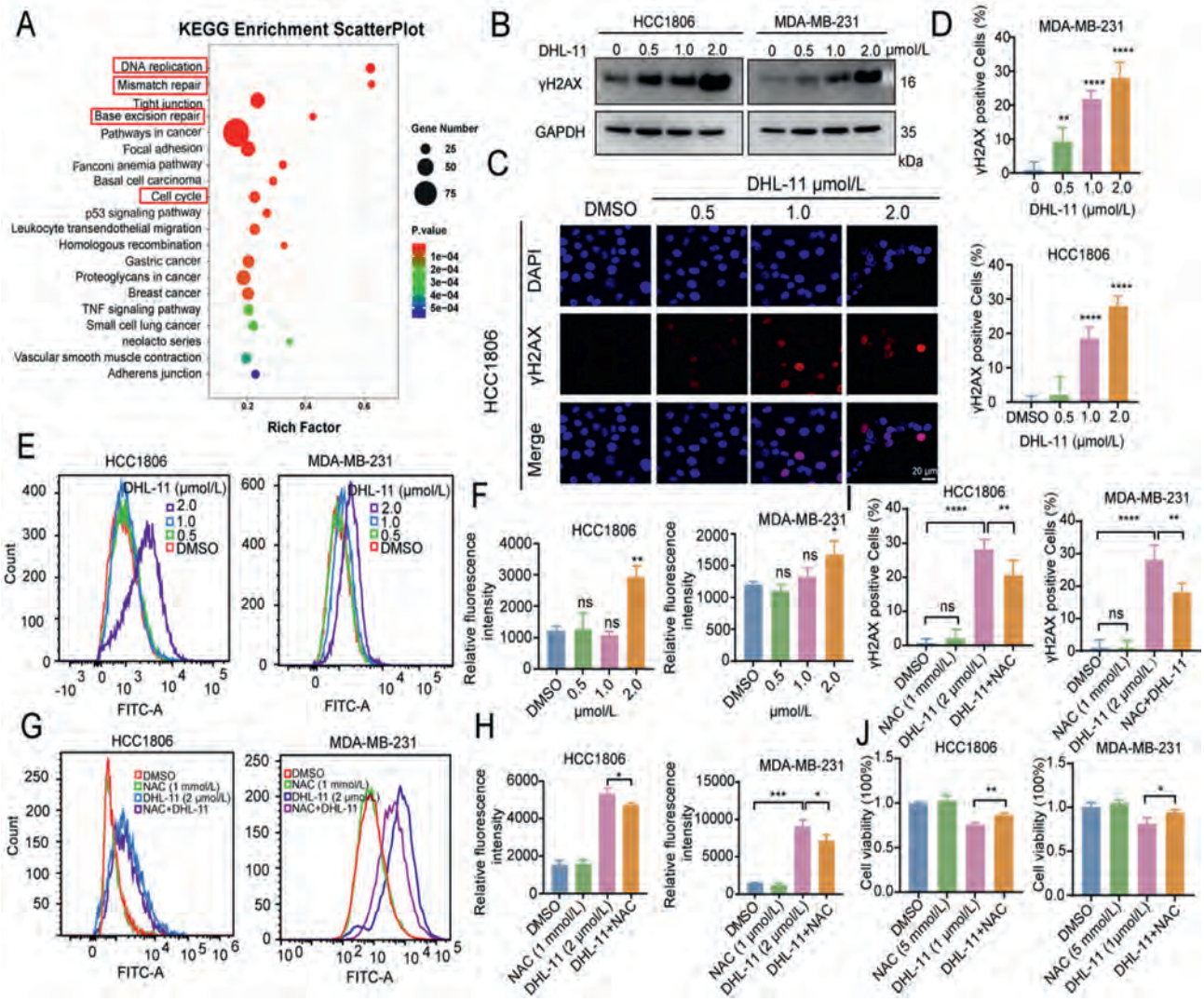

Figure 4 DHL-11 induces DNA damage in TNBC cells by increasing ROS levels. (A) KEGG annotation analysis of the DEGs in HCC1806 cells treated with DHL-11. (B) Western blot assay for detection of γH2AX protein levels after treatment with different concentrations of DHL-11 for 48 h. GAPDH was used as the loading control. (C) Immunofluorescence staining analysis of γH2AX levels. Scale bar: 20 μm. (D) Quantification of the proportion of γH2AX-positive cells. (E) After MDA-MB-231 and HCC1806 cells were treated with DHL-11 for 24 h, intracellular ROS levels were detected using flow cytometry. (F) Quantification of the relative ROS levels. (G) Flow cytometry was used to detect the intracellular ROS levels after treatment with DHL-11 (1 μmol/L) or NAC (1 mmol/L) for 24 h in MDA-MB-231 and HCC1806 cells. (H) Quantification of the relative ROS levels. (I) Quantification of the proportion of γH2AX-positive cells. (J) After pretreatment with NAC (5 mmol/L) for 6 h, TNBC cells were continued to treat with DHL-11 (1 μmol/L) for 48 h, and cell viability was detected *via* the SRB assay. Data are presented as mean ± SD ($n = 3$). $^{*}P < 0.05$, $^{**}P < 0.01$, $^{***}P < 0.001$ and $^{****}P < 0.0001$; ns, no statistically significant difference.

To elucidate the mechanism by which DHL-11 reduces IMPDH2 protein levels, we first measured the mRNA levels of IMPDH2 and found that DHL-11 had no effect on these levels (Fig. 6G). The proteasome inhibitor MG132 effectively blocked the degradation of IMPDH2 induced by DHL-11 in MDA-MB-231 and HCC1806 cells, while the lysosome inhibitor NH_4Cl was ineffective (Fig. 6H and I). Consistent with this, DHL-11 reduced the half-life of the IMPDH2 protein, as demonstrated by the cycloheximide (CHX) chase assay (Fig. 6J). Additionally, we measured the endogenous ubiquitination levels of IMPDH2 in MDA-MB-231 and HCC1806 cells after 24 h of treatment with DHL-11. The results showed that DHL-11 significantly increased the ubiquitination levels of IMPDH2 (Fig. 6K). Furthermore, FANCI has been shown to bind to and stabilize IMPDH2, thereby promoting growth in lung cancer cells[30]. Interestingly, we discovered that DHL-11 and FANCI may share the same binding site in the non-catalytic pocket of IMPDH2, as indicated by molecular docking analysis and AlphaFold 3 predictions (Fig. 6L and M, Supporting Information Fig. S5A). We then examined whether DHL-11 influences the interaction between FANCI and IMPDH2 using co-immunoprecipitation (Co-IP) assays. Notably, DHL-11 significantly reduced the protein-protein interaction between FANCI and IMPDH2 (Fig. 6N and O). Additionally, DHL-11 led to the downregulation of FANCI protein, likely due to the dissociation of the FANCI-IMPDH2 complex induced by DHL-11 (Fig. S5B). Our findings suggest that DHL-11 degrades both IMPDH2 and FANCI by disrupting their binding interactions.

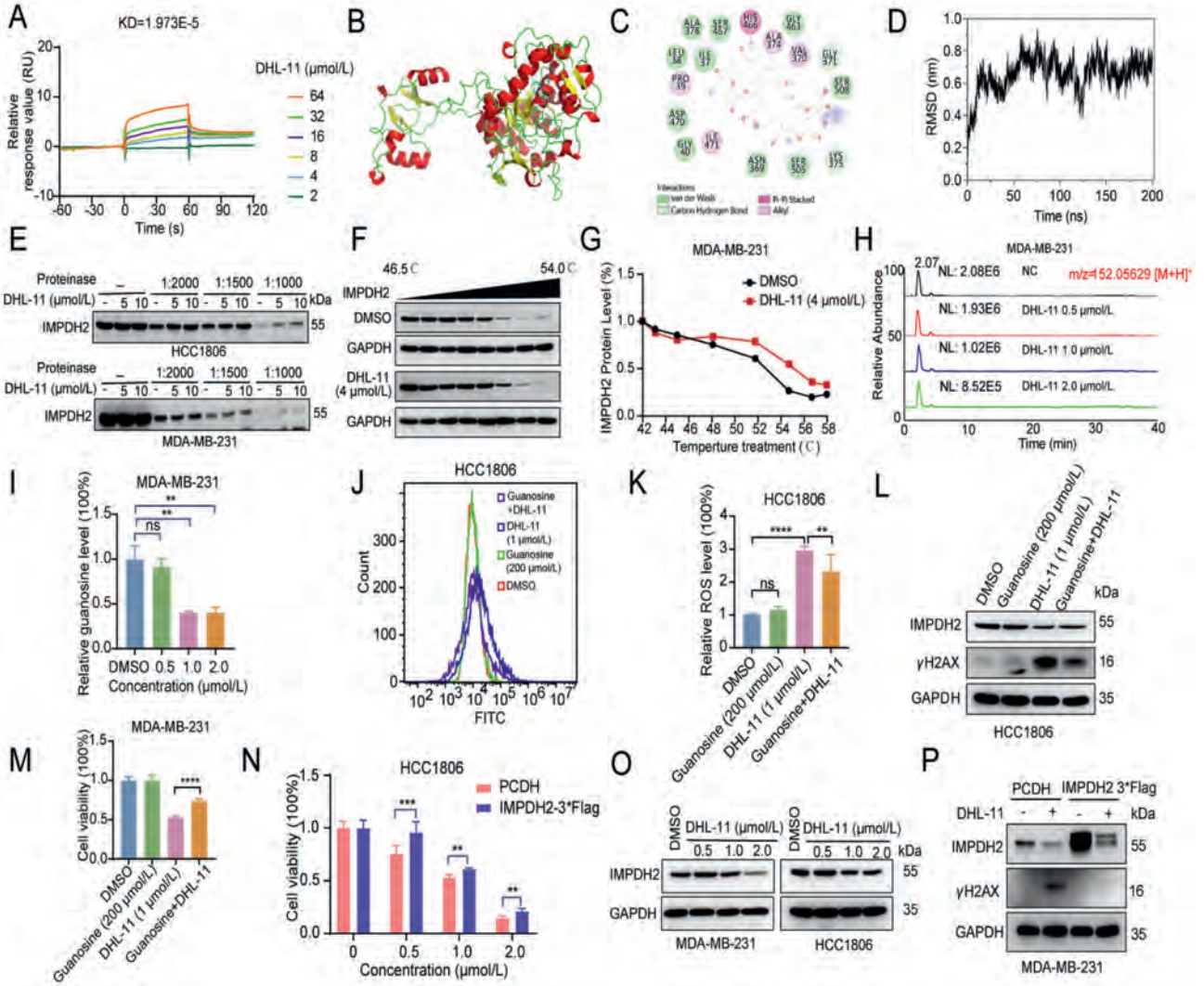

Figure 5 IMPDH2 is the target of DHL-11. (A) SPR analysis was used to confirm the binding between DHL-11 and IMPDH2. (B−D) Molecular docking and RMSD analysis of the binding of DHL-11 to IMPDH2. (E−G) DARTS (E) and CETSA (F) analysis of the binding between DHL-11 and IMPDH2. (H) High-performance liquid chromatography-mass spectrometry (HPLC−MS/MS) analysis of intracellular guanosine levels. The target peaks for the intracellular guanosine in $[M+H]^+$. (I) The quantitative analysis of the intracellular contents of guanosine. Data are presented as mean ± SD ($n = 3$). (J, K) Exogenous addition of guanine (200 μmol/L) into HCC1806 cells decreased the ROS level increase induced by DHL-11 (1 μmol/L, 24 h). Data are presented as mean ± SD ($n = 3$). (L) Exogenous addition of guanine into HCC1806 cells decreased the γH2AX level increase induced by DHL-11 (1 μmol/L, 48 h). (M) Exogenous addition of guanine partially rescues the cell viability loss caused by DHL-11. Data are presented as mean ± SD ($n = 5$). (N) Overexpression of IMPDH2 effectively inhibits DHL-11-induced antitumor activity. The values were normalized to their respective concentrations of 0 μmol/L and set as 100%. Data are presented as mean ± SD ($n = 5$). (O, P) DHL-11 reduces cellular exogenous and endogenous IMPDH2 protein levels. Data are representative of three independent experiments. GAPDH was used as the internal control. $^{**}P < 0.01$, $^{***}P < 0.001$ and $^{****}P < 0.0001$; ns, no statistically significant difference.

Furthermore, we assessed cell viability following treatment with DHL-11 and MPA. The results showed that DHL-11 has a lower IC_{50} than MPA in both the MDA-MB-231 and HCC1806 cell lines (Fig. 6P and Q), and DHL-11 induces more DNA damage compared to MPA (Fig. 6R). These findings suggest that DHL-11 binds to the non-catalytic domain of IMPDH2, while MPA interacts with the enzymatic activity domain of the same protein. As a novel IMPDH2 degrader, DHL-11 disrupts the interaction between FANCI and IMPDH2. Thus, DHL-11 and MPA inhibit IMPDH2 through distinct mechanisms.

3.6. IMPDH2-FANCI axis is a therapeutic target in TNBC

By analyzing the TCGA database, we found that the expression of IMPDH2 is significantly elevated in breast cancer tissues compared to normal breast tissues (Fig. 7A). Furthermore, patients with higher levels of IMPDH2 expression exhibited lower overall survival rates (Fig. 7B). A previous study indicated that IMPDH2 is highly expressed in breast cancer and is likely associated with poor prognosis[25]. We collected breast cancer tissues and adjacent normal tissues from TNBC patients to assess the expression of

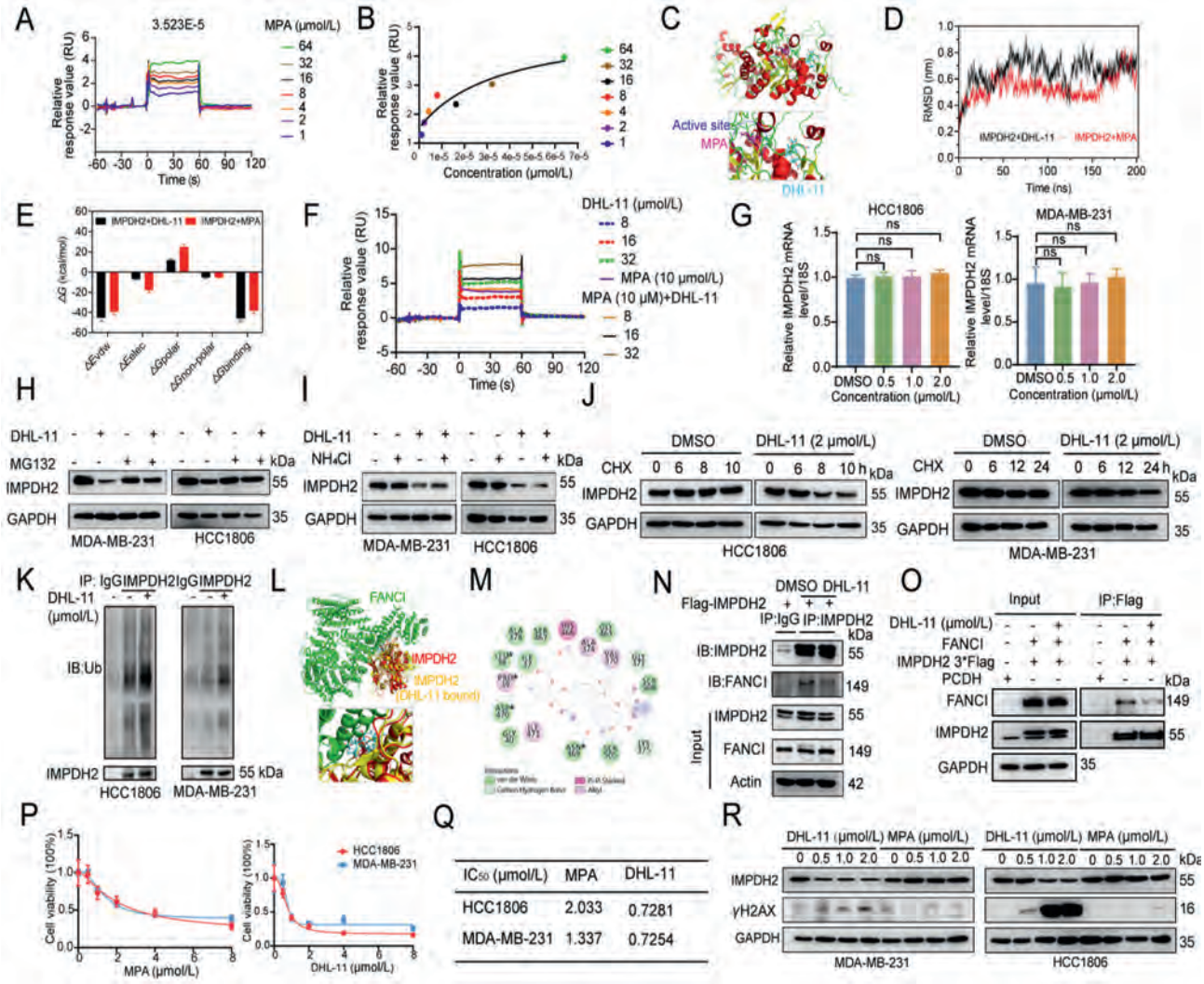

Figure 6 DHL-11 increases IMPDH2 protein degradation by binding the non-catalytic domain of IMPDH2. (A, B) SPR analysis was used to confirm the binding between MPA and IMPDH2. (C−E) Molecular docking analyzed the binding sites of DHL-11 and MPA to IMPDH2. (F) Competitive binding analysis of DHL-11 and MPA to IMPDH2. (G) The qRT-PCR assay was used to detect the changes in *IMPDH2* mRNA levels in TNBC cells after DHL-11 treatment. ns, no statistically significant difference. Data are presented as mean ± SD ($n = 3$). (H, I) DHL-11 degrades IMPDH2 *via* proteasome rather than lysosome. (J) DHL-11 shortens the half-life of the IMPDH2 protein. (K) The endogenous ubiquitination levels of IMPDH2 were detected after 24 h of DHL-11 treatment in the MDA-MB-231 and HCC1806 cells. (L) Docking analysis revealed DHL-11 binding to the interface of IMPDH2, which interacts with FANCI, disrupting the interaction between FANCI and IMPDH2. (M) Residues of IMPDH2 labeled with * represent direct interactions between IMPDH2 and both DHL-11 and FANCI. (N, O) DHL-11 disrupts the binding between IMPDH2 and FANCI through immunoprecipitation analysis. (P, Q) The IC_{50} values of DHL-11 and MPA in TNBC cells. Data are presented as mean ± SD ($n = 5$). (R) γH2AX and IMPDH2 levels were detected in TNBC cells after treatment with DHL-11 or MPA.

IMPDH2 protein. Our analysis confirmed that IMPDH2 expression was low in normal breast tissues but significantly elevated in TNBC tissues (Fig. 7C and D). In addition, we measured the expression levels of IMPDH2 in multiple breast cancer cell lines and showed that IMPDH2 expression was elevated in TNBC cells (Fig. S5C). Subsequently, we knocked down IMPDH2 in HCC1806 and MDA-MB-231 cells (Fig. S5D), observing that this knockdown significantly inhibited colony formation and cell proliferation (Fig. 7E and F, Fig. S5E and S5F). Consistently, IMPDH2 knockdown resulted in G2/M phase arrest (Fig. 7G and H, Fig. S5G and S5H), an accumulation of ROS (Fig. 7I and J, Fig. S5I and S5J), and increased levels of γH2AX (Fig. 7K) in TNBC cells. Analysis of the TCGA database revealed that FANCI is highly expressed in TNBC tissues, and elevated FANCI expression correlates with poorer prognosis (Fig. 7L and M). Knockdown of FANCI reduced IMPDH2 protein levels, significantly inhibited TNBC cell proliferation, and caused the accumulation of intracellular ROS (Fig. 7N−Q, Fig. S5K−S5N). These results suggest that the FANCI−IMPDH2 axis may be a potential therapeutic target in TNBC.

3.7. DHL-11 inhibits the growth of patient-derived TNBC organoids and xenograft tumors

To evaluate the potential therapeutic effects of DHL-11 on TNBC patients, we established patient-derived organoids (PDOs) to test

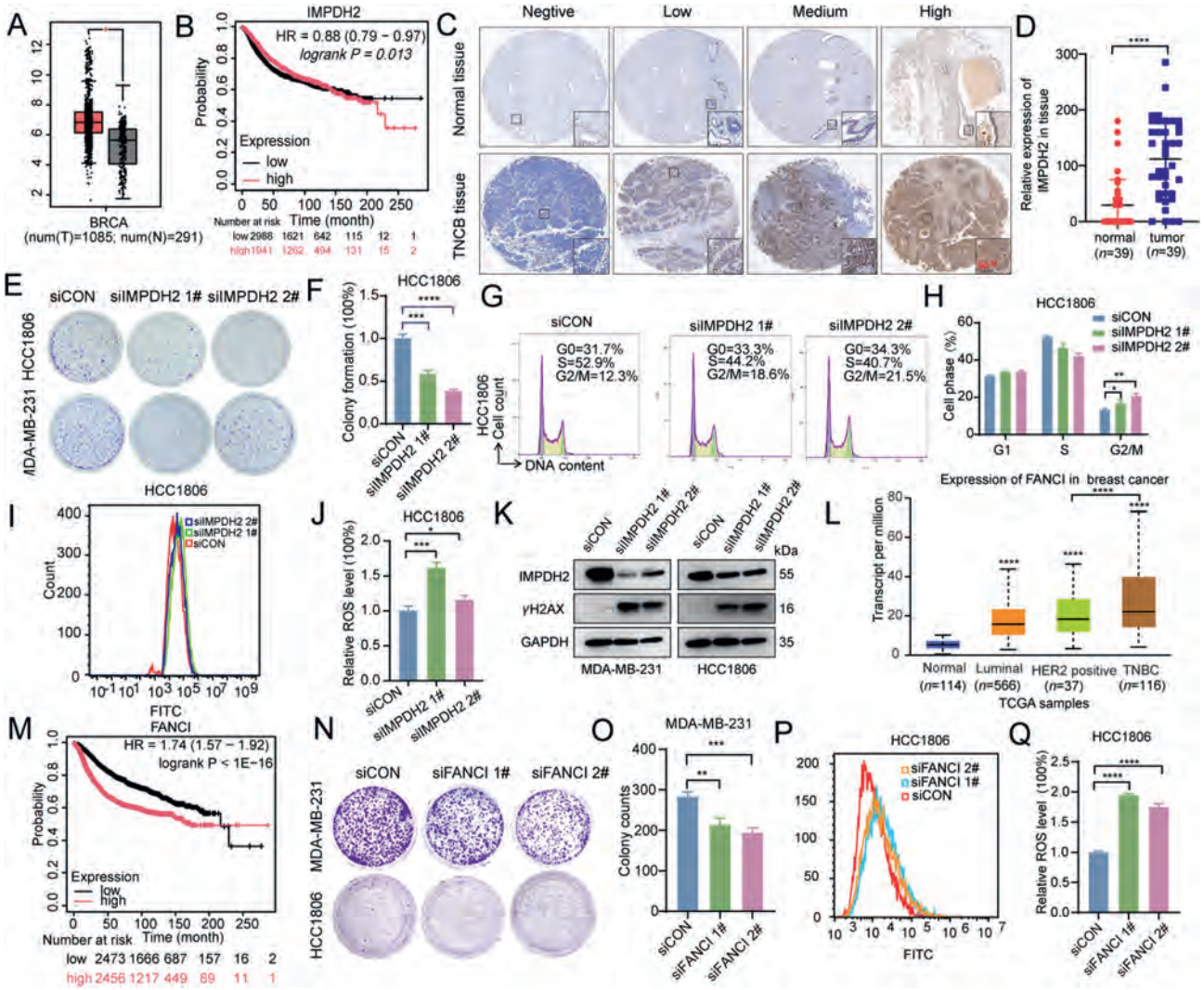

Figure 7 IMPDH2 is a therapeutic target in TNBC. (A, B) IMPDH2 is highly expressed in breast cancer tissues, and higher level of IMPDH2 resulted in lower overall survival rate. (C, D) Representative images of IMPDH2 expression in TNBC tissues and normal tissues (NT) by immunohistochemistry analysis. Following sectioning of all tissue samples ($n = 39$), the IMPDH2 positivity rate in each specimen was quantified and scored based on staining intensity criteria. Scale bar: 50 μm. (E) Representative images of colony formation in MAD-MB-231 and HCC1806 cells after IMPDH2 knockdown. (F) The quantification data for (E). (G) Cell cycle distribution was measured by FACS in HCC1806 cell lines after knockdown of IMPDH2. (H) The quantification data for (G). (I) ROS levels were measured by FACS in HCC1806 cells after knockdown of IMPDH2. (J) The quantification data for (I). (K) The levels of γH2AX protein were detected by Western blot analysis after knockdown of IMPDH2. (L, M) FANCI is highly expressed in breast cancer and correlated with poor prognosis in breast cancer. (N) Representative images of colony formation in MAD-MB-231 and HCC1806 cells after FANCI knockdown. (O) The quantification data for (N). (P) ROS levels were measured by FACS in HCC1806 cells after knockdown of FANCI. (Q) The quantification data for (P). Data are presented as mean ± SD ($n = 3$). Data are representative of three independent experiments. GAPDH was used as the internal control. $^{*}P < 0.05$, $^{**}P < 0.01$, $^{***}P < 0.001$ and $^{****}P < 0.0001$; ns, no statistically significant difference.

the drug's efficacy *in vitro*. We observed that DHL-11 induced crumpling, fragmentation, and loss of original morphology in the PDOs (Fig. 8A, Supporting Information Fig. S6A). The IC_{50} values for DHL-11 were 0.15 μmol/L (23BC109), 0.73 μmol/L (23BC138), 0.44 μmol/L (24BC297), and >10 μmol/L (23BC171) (Fig. 8B, Fig. S6B). Further analysis revealed that the DHL-11-sensitive PDO (23BC109) exhibited higher IMPDH2 expression compared to the DHL-11-resistant PDO (23BC171), which showed lower levels of IMPDH2 (Fig. 8C). To assess the anti-tumor activity of DHL-11 *in vivo*, we established a xenograft model by transplanting HCC1806 cells into nude mice. The mice were administered either a vehicle or DHL-11 (3 mg/kg) *via* gavage every two days while monitoring tumor growth, volume, and body weight (Fig. 8D). The results indicated that DHL-11 significantly inhibited the growth of TNBC cells in *vivo* (Fig. 8E−G) without affecting the body weight of the mice (Fig. 8H). Importantly, DHL-11 demonstrated no significant hepatotoxicity or nephrotoxicity, as indicated by serum levels of creatinine (SCr), AST, and ALT (Fig. 8I). Furthermore, immunohistochemical analysis of tumor samples revealed that DHL-11 significantly reduced the expression levels of Ki-67, IMPDH2, and FANCI (Fig. 8J and K, Fig. S6C and S6D). These findings suggest

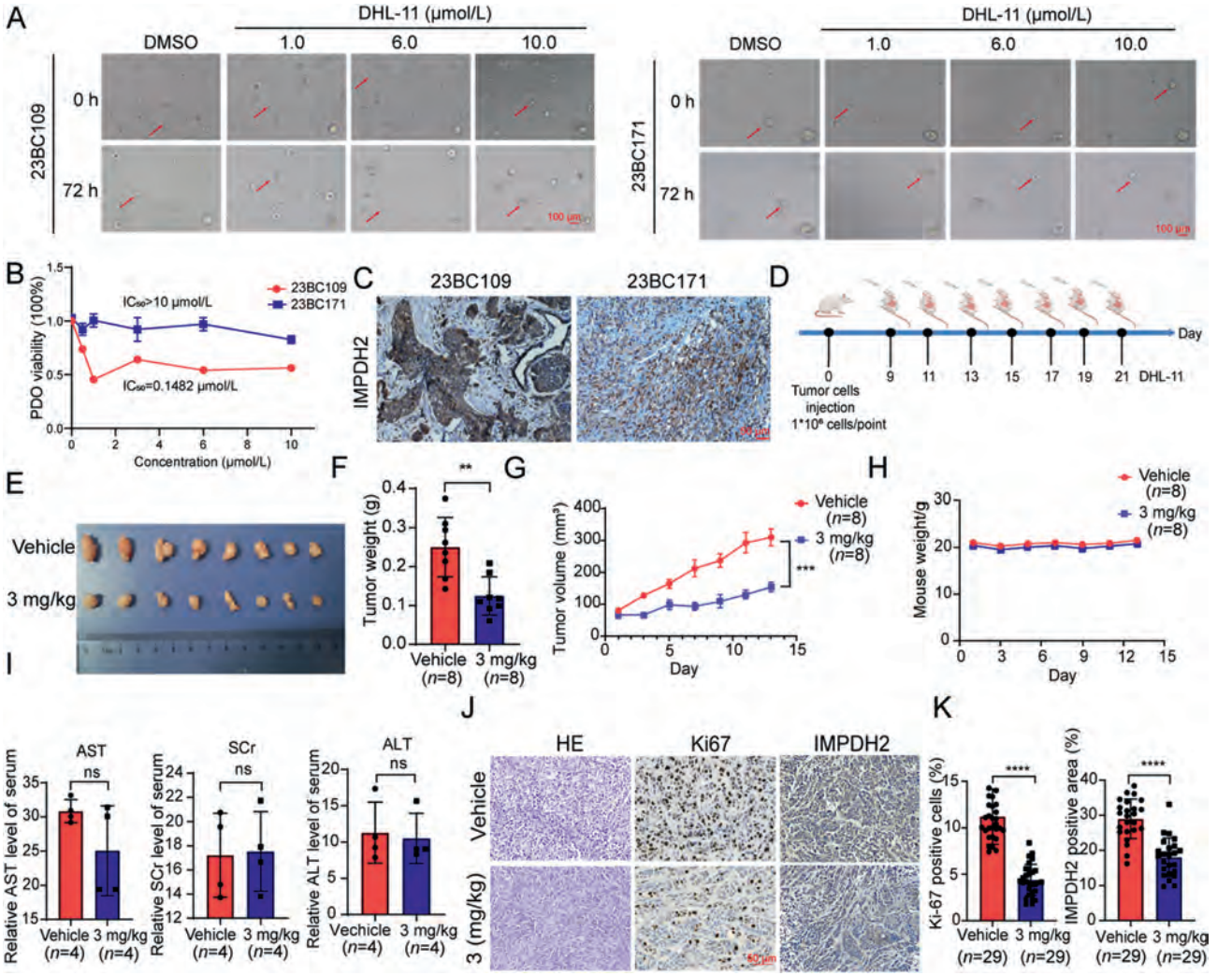

Figure 8 DHL-11 inhibits the growth of PDOs and xenograft tumors. (A, B) DHL-11 inhibits the growth of patient-derived TNBC organoids. Scale bar: 100 μm. Data are presented as mean ± SD ($n = 3$). (C) Immunohistochemistry assays were used to detect the expression levels of IMPDH2 in the two TNBC PDOs. Scale bar: 50 μm. (D) Schematic diagram of tumor model construction in nude mice and administration time and frequency. (E−H) DHL-11 inhibits the growth of xenograft tumors and has no effect on the body weight of mice. Data are presented as mean ± SD ($n = 8$). (I) DHL-11 has no significant hepatotoxicity and nephrotoxicity through analyzing the levels of alanine aminotransferase (ALT), aspartate aminotransferase (AST), and creatinine (SCr) in mouse serum. Data are presented as mean ± SD ($n = 4$). (J, K) Immunohistochemistry (IHC) analysis and quantification of Ki67-positive cells and IMDPH2 expression levels in tumour tissues (brown). All tumor tissues were sectioned into three experimental groups (8 slides per group) for HE staining and incubation with Ki67 and IMPDH2 antibodies, respectively. Immunohistochemistry slides were randomly selected for quantitative analysis of positive staining using standardized scoring criteria. Scale bar: 50 μm. Data are presented as mean ± SD ($n = 29$). Data are representative of three independent experiments. $^{**}P < 0.01$, $^{***}P < 0.001$ and $^{****}P < 0.0001$; ns, no statistically significant difference.

that DHL-11 effectively inhibits the growth of PDOs with high IMPDH2 expression and reduces both IMPDH2 levels and tumor growth in TNBC xenografts *in vivo*, all while maintaining a favorable safety profile.

3.8. The anti-TNBC activity of DHL-11 is dependent on the FANCI−IMPDH2 axis

To further elucidate the mechanism by which DHL-11 disrupts the FANCI−IMPDH2 interaction, we assessed the impact of FANCI knockdown on IMPDH2 stability and the anti-TNBC activity of DHL-11. Our results showed that the depletion of FANCI significantly reduced IMPDH2 protein levels and shortened its half-life (Fig. 9A), confirming that FANCI stabilizes IMPDH2 in TNBC. Consistent with this, the knockdown of FANCI reduced the sensitivity of TNBC cells to DHL-11-induced cytotoxicity (Fig. 9B and C). Conversely, the overexpression of FANCI rescued DHL-11-mediated cell death (Fig. 9D, Fig. S6E), further supporting DHL-11's role is dependent on FANCI. To identify the amino acids of IMPDH2 that bind to DHL-11, we designed and constructed two mutations by altering the presumed DHL-11-binding amino acids of IMPDH2, based on molecular docking analysis. IMPDH2-MUT1 is a mutant with alanine substitutions at five energy-contribution-critical residues (Ser467, Ile37, His504, Val370, Gly371) essential for interaction with DHL-11, while IMPDH2-MUT2 contains alanine replacements at four interface-

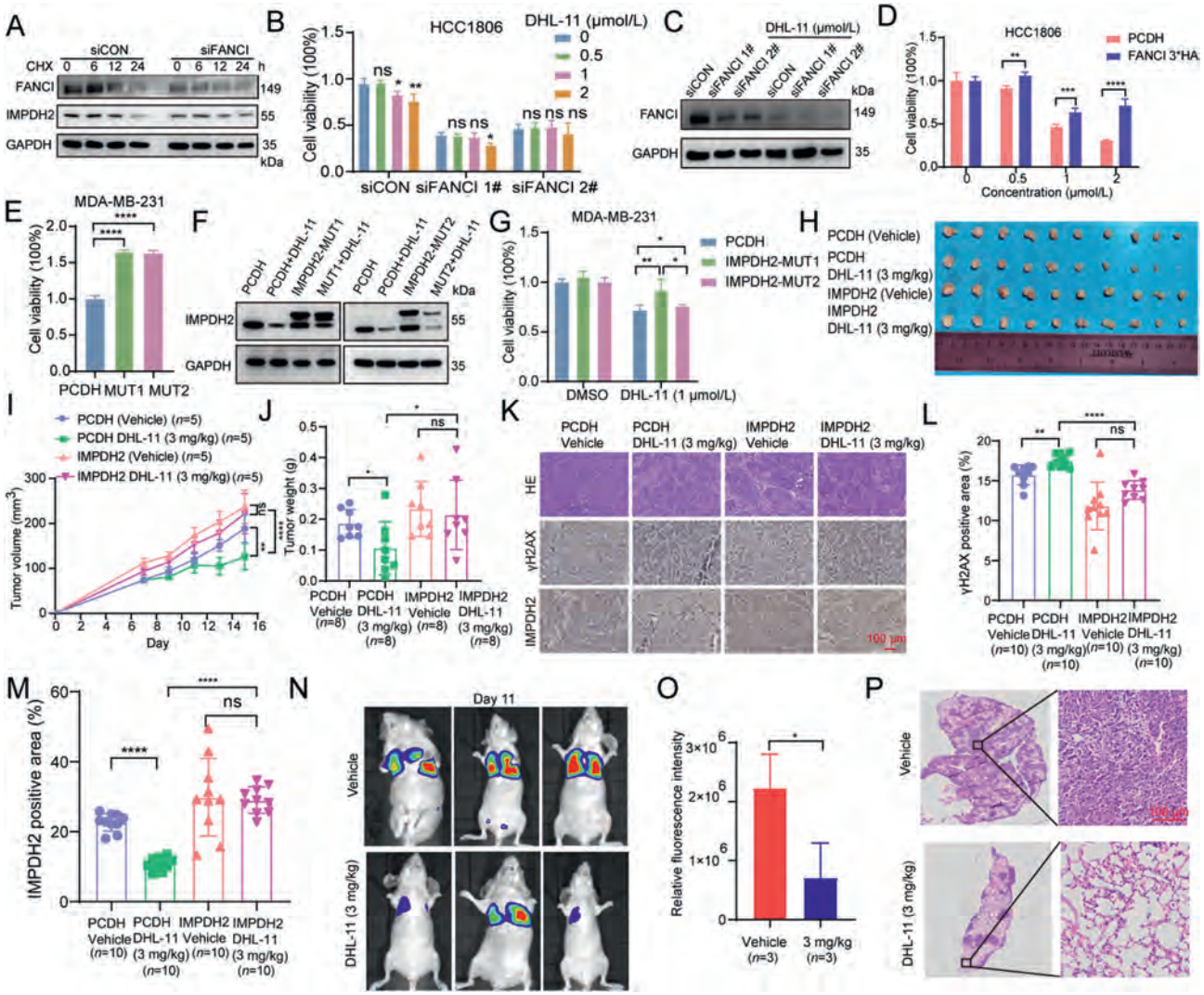

Figure 9 DHL-11 inhibits TNBC *via* the FANCI−IMPDH2 axis. (A) After knockdown of FANCI, cells were treated with CHX (50 μg/mL) for 6, 12, and 24 h. Subsequently, samples were collected to detect the protein levels of IMPDH2 and FANCI. (B) After knockdown of FANCI, cells were treated with DHL-11 for 48 h, and SRB assay was used to detect cell viability. Data are presented as mean ± SD ($n = 5$). (C) After knockdown of FANCI, cells were treated with DHL-11 for 48 h. Subsequently, FANCI protein levels were detected by Western blot analysis. (D) After overexpression of FANCI, cells were treated with DHL-11 for 48 h. Subsequently, the cell viability was detected by SRB assay. The values were normalized to their respective concentrations of 0 μmol/L and set as 100%. Data are presented as mean ± SD ($n = 5$). (E) Two IMPDH2 mutants (MUT1/MUT2) were stably expressed in MDA-MB-231 cells, and their effects on cell viability were measured by SRB assay. Data are presented as mean ± SD ($n = 5$). (F) Following 48-h treatment with DHL-11 in the cell lines that stably express IMPDH2-MUT1/MUT2 or PCDH (empty vector), IMDPH2 protein levels were detected by Western blot assay. The upper band is shown as the exogenous mutant IMPDH2 protein, and the lower band is the endogenous wild-type IMDPH2 protein. (G) Cell viability of MDA-MB-231 cells expressing IMPDH2-MUT1/MUT2 was detected using SRB assay following 48-h DHL-11 treatment. The values were normalized to their respective concentrations of DMSO and set as 100%. Data are presented as mean ± SD ($n = 5$). (H) Images of the tumors collected after mouse euthanasia. After establishing xenograft model using the HCC1806 cells stably overexpressing IMPDH2 in nude mice, DHL-11 (3 mg/kg) or vehicle control was administered *via* oral gavage for 7 times. (I, J) The quantitative data for tumor volume and tumor weight. Data are presented as mean ± SD ($n = 5$). (K−M) Immunohistochemistry (IHC) analysis and quantification of γH2AX-positive cells and IMDPH2 expression levels in tumour tissues (brown). All tumor tissues were sectioned into three experimental groups (10 slides per group) for HE staining and incubation with γH2AX and IMPDH2 antibodies, respectively, and the immunohistochemistry slides were randomly selected for quantitative analysis of positive staining using standardized scoring criteria. Scale bar: 100 μm. Data are presented as mean ± SD ($n = 10$). (N) The treated 4T1-luc cells were injected intravenously *via* tail vein into nude mice and observed for the luciferase signals after DHL-11 (3 mg/kg) or vehicle treatment. (O) The quantitative data for fluorescence intensity in mouse lungs. Data are presented as mean ± SD ($n = 3$). (P) H&E staining images of metastasis in lung sections and observation of metastasis in mice treated with or without DHL-11. Scale bar: 100 μm. Data are representative of three independent experiments. $^{*}P < 0.05$, $^{**}P < 0.01$, $^{***}P < 0.001$ and $^{****}P < 0.0001$; ns, no statistically significant difference.

overlapping residues (Leu38, Pro39, Asp470, Asn369) shared between DHL-11 and FANCI binding sites. We then established two cell lines overexpressing IMPDH2-MUT1 and MUT2, each tagged with a FLAG epitope. Both IMPDH2-MUT1 and MUT2 promoted cell proliferation (Fig. 9E), indicating that the mutations did not affect IMPDH2 stability or activity. Interestingly, DHL-11 failed to degrade the exogenous IMPDH2-MUT1 protein, whereas it continued to degrade the wild-type and exogenous IMPDH2-MUT2 proteins (Fig. 9F). SRB assays demonstrated that IMPDH2-MUT1 was more effective than IMPDH2-MUT2 in rescuing cells from DHL-11-mediated cell death (Fig. 9G). Additionally, Co-IP assays showed that DHL-11 could not disrupt the binding between FANCI and IMPDH2-MUT1 (Fig. S6F). These results strongly support the idea that IMPDH2-MUT1 disrupts the putative binding interface between IMPDH2 and DHL-11, indicating that the anti-cancer effects of DHL-11 rely on its direct interaction with key residues of IMPDH2-MUT1. To determine whether the antitumor activity of DHL-11 is dependent on IMPDH2 *in vivo*, we established a mouse xenograft model using HCC1806 cell lines that stably overexpress IMPDH2. Our data showed that the overexpression of IMPDH2 significantly abolished the inhibitory effects of DHL-11 on HCC1806-derived xenografts (Fig. 9H−J) and that IMPDH2 overexpression attenuated DHL-11-induced DNA damage (Fig. 9K−M). These findings provide strong evidence that DHL-11 mediates DNA damage through the degradation of IMPDH2 to inhibit tumorigenesis *in vivo*. The lungs serve as a primary metastatic site for TNBC, acting as the first major capillary bed encountered by TNBC cells that escape into the bloodstream. We also established a lung metastasis model through tail vein injection using the mouse-derived TNBC cell line 4T1-luc. We then administered DHL-11 (3 mg/kg) *via* oral gavage to observe its effects on migration and metastasis. The results indicate that DHL-11 effectively inhibited the lung metastasis of 4T1 cells in nude mice (Fig. 9N−P). These *in vivo* data further support the potential of DHL-11 as an anti-metastatic agent.

4. Discussion

In this study, we identified the limonoid DHL-11, derived from the traditional Chinese herb *Munronia Henryi*, as an effective inhibitor of cell proliferation, migration, and survival in HCC1806 and MDA-MB-231 cells. DHL-11 blocks the cell cycle in TNBC at the G2/M phase and induces apoptosis. Additionally, DHL-11 inhibits the growth of HCC1806-derived xenograft tumors in mice without causing significant hepatotoxicity or nephrotoxicity, and it suppresses the growth of PDOs *in vitro*. These findings indicate that DHL-11 exhibits robust anti-TNBC activity both *in vivo* and *in vitro*, suggesting a potential expansion of clinical applications for the traditional Chinese medicine *Munronia Henryi*.

The mechanistic study demonstrates that DHL-11 binds to the IMPDH2 protein, thereby inhibiting guanine synthesis. The exogenous addition of guanine and the overexpression of IMPDH2 effectively reverse the antitumor activity and DNA damage induced by DHL-11. DHL-11 accelerates the degradation of the IMPDH2 protein by competitively binding to its non-catalytic pocket, which results in decreased stability of both FANCI and IMPDH2. Both FANCI and IMPDH2 are highly expressed in breast cancer, with elevated levels correlating with lower overall survival rates. Consistently, the knockdown of IMPDH2 significantly inhibits cell proliferation and induces ROS and DNA damage. Thus, DHL-11 is distinct from other IMPDH2 inhibitors, including MPA, as it specifically binds to IMPDH2, circumventing the limitations of other inhibitors that non-specifically target IMPDH1. As anticipated, DHL-11 demonstrates better efficacy and safety compared to MPA. Further clinical investigations are warranted to determine whether DHL-11 and MPA can be utilized in the treatment of TNBC.

Wang et al.[39] discovered that IMPDH2 is highly expressed in breast cancer, and survival analysis indicated that elevated levels of IMPDH2 are associated with cancer progression and poor prognosis in TNBC. Additionally, Espinar et al.[58] demonstrated that IMPDH2 in TNBC is preferentially enriched in chromatin compared to other isoforms, suggesting its potential as a novel therapeutic target for TNBC in the future. While MPA, a traditional inhibitor of IMPDH2, is currently used clinically as an immunosuppressant, this study has identified its anti-TNBC effects. The potential for repurposing MPA as an established drug in a new context, integrated into TNBC treatment strategies, warrants further clinical investigation. In this study, the combination of DHL-11 and MPA was evaluated for treating TNBC cells, and the results revealed that the two agents did not produce a synergistic effect (Fig. S6G and S6H). Additionally, FANCI can bind to IMPDH2, stabilizing the IMPDH2 protein[30]. Recent studies reported that IMPDH2 or FANCI interacts with PARP1 to regulate PARP1 activity in breast cancer[22,50]. Upon induction of DNA damage, IMPDH2 is recruited to chromatin to interact with PARP1, and this interaction modulates NAD + availability, thus controlling PARP1 activity; unlike IMPDH2, FANCI promotes the nuclear localization and functionality of PARP1[22]. Intriguingly, DHL-11 reduced the protein levels of both IMPDH2 and FANCI, which caused amplified DNA damage. Therefore, combining DHL-11 with PARP inhibitors may synergistically induce DNA damage to inhibit TNBC growth, which awaits further exploration[58]. Therefore, the potential synergistic anti-TNBC effect of combining DHL-11 with PARP inhibitors warrants further exploration.

Tumor cells require rapid DNA synthesis for continuous proliferation, and the depletion of nucleotides poses a catastrophic threat to their survival. Currently, 5-fluorouracil, a chemotherapeutic agent used in clinical practice, exerts its antitumor effects effectively by inhibiting thymidylate synthase. IMPDH2, the rate-limiting enzyme in guanine synthesis, is highly expressed in various malignant tumors, including breast cancer. In colorectal cancer, IMPDH2 enhances cell invasion, migration, and epithelial-to-mesenchymal transition (EMT) by activating the PI3K/AKT/mTOR signaling pathway[25]. In non-small cell lung cancer, it promotes EMT through the Wnt/β-catenin signaling pathway[56]. Additionally, IMPDH2 contributes to glioblastoma development by inducing aberrant karyorrhexis[59]. Therefore, IMPDH2 represents a promising target for anticancer drug discovery. Our research has demonstrated that IMPDH2 is overexpressed in TNBC, and its depletion or inhibition significantly reduces the viability of TNBC cells.

Guanosine is a vital nucleotide involved in numerous cellular biological processes and exhibits significant antioxidant properties, likely due to its direct scavenging activity[60,61]. Previous studies have shown that guanosine can prevent the disruption of mitochondrial membrane potential caused by oxygen−glucose deprivation (OGD) in hippocampal slices, thereby protecting cells from oxidative damage resulting from compromised mitochondrial function[62]. Furthermore, Courtes et al.[63] observed that guanosine reduced mitochondrial swelling in the presence of Ca^{2+}, as well as decreased ROS production and hydrogen peroxide levels. Additionally, guanosine enhanced the activity of manganese superoxide

dismutase, oxidative phosphorylation, and the tricarboxylic acid cycle. These findings underscore the importance of guanosine in maintaining intracellular ROS homeostasis.

High levels of ROS are well-known to cause DNA damage and apoptosis[64,65]. The presence of ROS in the cytoplasm triggers the release of cytochrome *c* and activates the JNK and p38−MAPK pathways[65]. Consistent with this, our experimental results indicate that DHL-11 inhibits DNA synthesis, promotes the accumulation of intracellular ROS, and increases DNA damage by degrading IMPDH2 in TNBC cells. The antioxidant NAC and the overexpression of IMPDH2 mitigate the antitumor activity and DNA damage induced by DHL-11, suggesting that DHL-11 functions as an inducer of ROS and DNA damage for the treatment of TNBC.

Previous studies have reported that the knockdown of IMPDH2 suppresses NF-κB activation by decreasing the protein levels of p-IKBα and p-IKKα/β[31]. Interestingly, we also observed that either the knockdown of IMPDH2 or treatment with DHL-11 significantly reduces the levels of p-IKBα and p-IKKα/β. Furthermore, treatment with DHL-11 following IMPDH2 knockdown synergistically inhibits the activation of the NF-κB signaling pathway (Fig. S6I). These findings suggest that DHL-11 may exhibit anti-inflammatory effects by blocking NF-κB activation. However, the underlying mechanism of IMPDH2-induced NF-κB activation remains unclear and requires further investigation.

5. Conclusions

DHL-11 effectively targets and degrades IMPDH2 by disrupting the interaction between FANCI and IMPDH2. This disruption leads to increased replication stress, accumulation of ROS, DNA damage, and ultimately triggers apoptosis in TNBC cells (Fig. 1). This study highlights DHL-11 as a promising natural product for the treatment of TNBC and may facilitate the clinical application of limonoids.

Acknowledgements

This work was supported by Noncommunicable Chronic Diseases-National Science and Technology Major Project (2023ZD0502200, China), National Natural Science Foundation of China (U2102203, 82430084, 82404666, 82260691, 82260487, 82360687, 82302957). Biomedical Projects of Yunnan Key Science and Technology Program (202302AA310046, China), Yunnan Fundamental Research Projects (Major project: 202501AS070023, 202201BC070002; General project: 202401AT070171; 202401CF070054, China). Yunnan Academician Expert Workstation (202505AF350058, China). The Innovative Research Team of Yunnan Province (202405AS350016, China). Yunnan Revitalization Talent Support Program (XDYC-QNRC-2023-0177, XDYC-QNRC-2023-0178, China). First-Class Discipline Team of Kunming Medical University (2024XKTDPY16, China). Guizhou Provincial Science and Technology Project (ZK [2022]393, China). Joint Special Funds for the Department of Science and Technology of Yunnan Province-Kunming Medical University (202501AY070001-027, China).

Author contributions

Yu Zhu conducted the experiments and drafted the manuscript. Zhibi Zhang performed the molecular docking simulation predictions. Xueqin Dai constructed the organoid models. Wenjing Liu and Jian Sun developed the nude mouse xenograft model. Jialing Liu prepared for the SPR experiments. Yuxin Zhao assisted in the construction of overexpression plasmids. Wenlong Ren contributed to the experimental design. Chenglong Pan analyzed the IHC results. Ying Yan reviewed and edited the manuscript. Zhongmei Zhou provided technical support. Longlong Zhang reviewed and edited the manuscript. Ceshi Chen supervised, reviewed, and edited the manuscript.

Conflicts of interest

The authors declare no competing interests.

Supporting information

Supporting information to this article can be found online at https://doi.org/10.1016/j.apsb.2025.10.031.

References

1. Nolan E, Lindeman GJ, Visvader JE. Deciphering breast cancer: from biology to the clinic. *Cell* 2023;**186**:1708−28.
2. Waks AG, Winer EP. Breast cancer treatment: a review. *JAMA* 2019; **321**:288−300.
3. Bray F, Laversanne M, Sung H, Ferlay J, Siegel RL, Soerjomataram I, et al. Global cancer statistics 2022: GLOBOCAN estimates of incidence and mortality worldwide for 36 cancers in 185 countries. *CA Cancer J Clin* 2024;**74**:229−63.
4. Thennavan A, Beca F, Xia Y, Garcia-Recio S, Allison K, Collins LC, et al. Molecular analysis of TCGA breast cancer histologic types. *Cell Genom* 2021;**1**:100067.
5. Wang Y, Min J, Deng X, Feng T, Hu H, Guo X, et al. Discovery of novel covalent selective estrogen receptor degraders against endocrine-resistant breast cancer. *Acta Pharm Sin B* 2023;**13**:4963−82.
6. Wu Q, Nie DY, Ba-alawi W, Ji Y, Zhang Z, Cruickshank J, et al. PRMT inhibition induces a viral mimicry response in triple-negative breast cancer. *Nat Chem Biol* 2022;**18**:821−30.
7. Zhang J, Zhang Z, Huang Z, Li M, Yang F, Wu Z, et al. Isotoosendanin exerts inhibition on triple-negative breast cancer through abrogating TGF-β-induced epithelial−mesenchymal transition *via* directly targeting TGFβR1. *Acta Pharm Sin B* 2023;**13**:2990−3007.
8. Son Y, Cheong YK, Kim NH, Chung HT, Kang DG, Pae HO. Mitogen-activated protein kinases and reactive oxygen species: how can ROS activate MAPK pathways?. *J Signal Transduct* 2011;**2011**:792639.
9. Jin SY, Lee HS, Kim EK, Ha JM, Kim YW, Bae S. Reactive oxygen species and PI3K/Akt signaling in cancer. *Free Radic Biol Med* 2014; **75**:S34−5.
10. Kansanen E, Kuosmanen SM, Leinonen H, Levonen AL. The Keap1−Nrf2 pathway: mechanisms of activation and dysregulation in cancer. *Redox Biol* 2013;**1**:45−9.
11. Corzo CA, Cotter MJ, Cheng P, Cheng F, Kusmartsev S, Sotomayor E, et al. Mechanism regulating reactive oxygen species in tumor-induced myeloid-derived suppressor cells. *J Immunol* 2009;**182**:5693−701.
12. Nagaraj S, Gupta K, Pisarev V, Kinarsky L, Sherman S, Kang L, et al. Altered recognition of antigen is a mechanism of $CD8^+$ T cell tolerance in cancer. *Nat Med* 2007;**13**:828−35.
13. Randerath K, Randerath E, Smith CV, Chang J. Structural origins of bulky oxidative DNA adducts (type II I-compounds) as deduced by oxidation of oligonucleotides of known sequence. *Chem Res Toxicol* 1996;**9**:247−54.
14. Sun X, Wang Y, Ji K, Liu Y, Kong Y, Nie S, et al. NRF2 preserves genomic integrity by facilitating ATR activation and G2 cell cycle arrest. *Nucleic Acids Res* 2020;**48**:9109−23.

15. Reis J, Gorgulla C, Massari M, Marchese S, Valente S, Noce B, et al. Targeting ROS production through inhibition of NADPH oxidases. *Nat Chem Biol* 2023;**19**:1540−50.
16. Alter BP, Giri N, Savage SA, Rosenberg PS. Cancer in the National cancer Institute inherited bone marrow failure syndrome cohort after fifteen years of follow-up. *Haematologica* 2018;**103**: 30−9.
17. Wang R, Wang S, Dhar A, Peralta C, Pavletich NP. DNA clamp function of the monoubiquitinated Fanconi anaemia ID complex. *Nature* 2020;**580**:278−82.
18. Alcón P, Shakeel S, Chen ZA, Rappsilber J, Patel KJ, Passmore LA. FANCD2−FANCI is a clamp stabilized on DNA by monoubiquitination of FANCD2 during DNA repair. *Nat Struct Mol Biol* 2020;**27**:240−8.
19. Smogorzewska A, Matsuoka S, Vinciguerra P, McDonald ER, Hurov KE, Luo J, et al. Identification of the FANCI protein, a monoubiquitinated FANCD2 paralog required for DNA repair. *Cell* 2007; **129**:289−301.
20. Hou Y, Li J, Yu A, Deng K, Chen J, Wang Z, et al. FANCI is associated with poor prognosis and immune infiltration in liver hepatocellular carcinoma. *Int J Med Sci* 2023;**20**:918−32.
21. Cai ZG, Duan YJ, Li W, Liu ZH, Gong ZJ, Hong S, et al. FANCI serve as a prognostic biomarker correlated with immune infiltrates in skin cutaneous melanoma. *Front Immunol* 2023;**14**:1295831.
22. Huang YZ, Sang MY, Xi PW, Xu RX, Cai MY, Wang ZW, et al. FANCI inhibition induces PARP1 redistribution to enhance the efficacy of PARP inhibitors in breast cancer. *Cancer Res* 2024;**84**: 3447−63.
23. Pua KH, Stiles DT, Sowa ME, Verdine GL. IMPDH2 is an intracellular target of the cyclophilin a and sanglifehrin A complex. *Cell Rep* 2017;**18**:432−42.
24. Colby TD, Vanderveen K, Strickler MD, Markham GD, Goldstein BM. Crystal structure of human type II inosine monophosphate dehydrogenase: implications for ligand binding and drug design. *Proc Natl Acad Sci U S A* 1999;**96**:3531−6.
25. Duan S, Huang W, Liu X, Liu X, Chen N, Xu Q, et al. IMPDH2 promotes colorectal cancer progression through activation of the PI3K/AKT/mTOR and PI3K/AKT/FOXO1 signaling pathways. *J Exp Clin Cancer Res* 2018;**37**:304.
26. Zou J, Han Z, Zhou L, Cai C, Luo H, Huang Y, et al. Elevated expression of IMPDH2 is associated with progression of kidney and bladder cancer. *Med Oncol* 2014;**32**:373.
27. Zhou L, Xia D, Zhu J, Chen Y, Chen G, Mo R, et al. Enhanced expression of IMPDH2 promotes metastasis and advanced tumor progression in patients with prostate cancer. *Clin Transl Oncol* 2014; **16**:906−13.
28. Xing Y, Yang H, Dai C, Qiu Z, Guan Y, Zhang L. Investigating the mechanism of ferroptosis induction by sappanone A in hepatocellular carcinoma: NRF2/xCT/GPX4 axis. *Eur J Pharmacol* 2024;**983**: 176965.
29. Ruan X, Xiong Y, Li X, Yang E, Wang J. Lower ratio of IMPDH1 to IMPDH2 sensitizes gliomas to chemotherapy. *Cancer Gene Ther* 2024;**31**:1081−9.
30. Zheng P, Li L. FANCI cooperates with IMPDH2 to promote lung adenocarcinoma tumor growth *via* a MEK/ERK/MMPs pathway. *OncoTargets Ther* 2020;**13**:451−63.
31. Liao LX, Song XM, Wang LC, Lv HN, Chen JF, Liu D, et al. Highly selective inhibition of IMPDH2 provides the basis of antineuroinflammation therapy. *Proc Natl Acad Sci U S A* 2017;**114**: E5986−94.
32. Ling J, Kumar R. Crosstalk between NFκB and glucocorticoid signaling: a potential target of breast cancer therapy. *Cancer Lett* 2012;**322**:119−26.
33. Cuny GD, Suebsuwong C, Ray SS. Inosine-5′-monophosphate dehydrogenase (IMPDH) inhibitors: a patent and scientific literature review (2002−2016). *Expert Opin Ther Pat* 2017;**27**:677−90.
34. Sintchak MD, Fleming MA, Futer O, Raybuck SA, Chambers SP, Caron PR, et al. Structure and mechanism of inosine monophosphate dehydrogenase in complex with the immunosuppressant mycophenolic acid. *Cell* 1996;**85**:921−30.
35. Klangjorhor J, Chaiyawat P, Teeyakasem P, Sirikaew N, Phanphaisarn A, Settakorn J, et al. Mycophenolic acid is a drug with the potential to be repurposed for suppressing tumor growth and metastasis in osteosarcoma treatment. *Int J Cancer* 2019;**146**: 3397−409.
36. Aghazadeh S, Yazdanparast R. Mycophenolic acid potentiates HER2-overexpressing SKBR3 breast cancer cell line to induce apoptosis: involvement of AKT/FOXO1 and JAK2/STAT3 pathways. *Apoptosis* 2016;**21**:1302−14.
37. Pan H, Hu Q, Wang J, Liu Z, Wu D, Lu W, et al. Myricetin is a novel inhibitor of human inosine 5′-monophosphate dehydrogenase with anti-leukemia activity. *Biochem Biophys Res Commun* 2016;**477**: 915−22.
38. He X, Cui J, Ma H, Abuduaini N, Huang Y, Tang L, et al. Berberrubine is a novel and selective IMPDH2 inhibitor that impairs the growth of colorectal cancer. *Biochem Pharmacol* 2023;**218**:115868.
39. Wang W, Wu Y, Chen S, Liu X, He J, Wang S, et al. Shikonin is a novel and selective IMPDH2 inhibitor that target triple-negative breast cancer. *Phytother Res* 2020;**35**:463−76.
40. Davies NM, Grinyo J, Heading R, Maes B, Meier-Kriesche HU, Oellerich M. Gastrointestinal side effects of mycophenolic acid in renal transplant patients: a reappraisal. *Nephrol Dial Transplant* 2007; **22**:2440−8.
41. Zhang JC, Liao Q, Shen L, Wu J. Twenty-five limonoids from the Hainan mangrove, *Xylocarpus granatum*. *Bioorg Chem* 2020;**100**: 103903.
42. Wang GK, Sun YP, Jin WF, Yu Y, Zhu JY, Liu JS. Limonoids from *Swietenia macrophylla* and their antitumor activities in A375 human malignant melanoma cells. *Bioorg Chem* 2022;**123**:105780.
43. Sandhir R, Khurana M, Singhal NK. Potential benefits of phytochemicals from *Azadirachta indica* against neurological disorders. *Neurochem Int* 2021;**146**:105023.
44. Lam LK, Hasegawa S. Inhibition of benzo[*a*]pyrene-induced forestomach neoplasia in mice by citrus limonoids. *Nutr Cancer* 1989;**12**: 43−7.
45. Liu HB, Zhang CR, Dong SH, Dong L, Wu Y, Yue JM. Limonoids and triterpenoids from the seeds of *Melia azedarach*. *Chem Pharm Bull (Tokyo)* 2011;**59**:1003−7.
46. Pooladanda V, Thatikonda S, Bale S, Pattnaik B, Sigalapalli DK, Bathini NB, et al. Nimbolide protects against endotoxin-induced acute respiratory distress syndrome by inhibiting TNF-alpha mediated NF-kappaB and HDAC-3 nuclear translocation. *Cell Death Dis* 2019;**10**:81.
47. Yan Y, Wang D, Zhang X, Peng M, Yan X, Guo Y, et al. Anti-TMV activity and effects of three prieurianin-type limonoids from *Munronia henryi*. *Pestic Biochem Physiol* 2022;**184**:105108.
48. Tan QG, Luo XD. Meliaceous limonoids: chemistry and biological activities. *Chem Rev* 2011;**111**:7437−522.
49. Nagini S, Nivetha R, Palrasu M, Mishra R. Nimbolide, a Neem limonoid, is a promising candidate for the anticancer drug arsenal. *J Med Chem* 2021;**64**:3560−77.
50. Bardia A, Mayer IA, Vahdat LT, Tolaney SM, Isakoff SJ, Diamond JR, et al. Sacituzumab Govitecan-hziy in refractory metastatic triple-negative breast cancer. *N Engl J Med* 2019;**380**:741−51.
51. Yan Y, Tang L, Hu J, Wang J, Adelakun TA, Yang D, et al. Munronin O, a potential activator for plant resistance. *Pestic Biochem Physiol* 2018;**146**:13−8.
52. Lai H, Liu C, Hou L, Lin W, Chen T, Hong A. TRPM8-regulated calcium mobilization plays a critical role in synergistic chemosensitization of Borneol on Doxorubicin. *Theranostics* 2020;**10**: 10154−70.
53. Wang TT, Zhang LL, Li FB, Zhang J, Zhang ZB, Mi DZ, et al. LN-439A, a novel BAP1 inhibitor, suppresses the growth of basal-like breast cancer by degrading KLF5. *Acta Pharmacol Sin* 2025;**46**: 715−27.
54. Ding XJ, Cai XM, Wang QQ, Liu N, Zhong WL, Xi XN, et al. Vitexicarpin suppresses malignant progression of colorectal cancer

through affecting c-Myc ubiquitination by targeting IMPDH2. *Phytomedicine* 2024;**132**:155833.
55. Wu Z, Wu QF, Yuan WL, Chen YH, Hu D, Deng DY, et al. Arthrocolins synergizing with fluconazole inhibit fluconazole-resistant *Candida albicans* by increasing riboflavin metabolism and causing mitochondrial dysfunction and autophagy. *Microbiol Spectr* 2023;**11**: e0405122.
56. Xu H, Ma H, Zha L, Li Q, Yang G, Pan H, et al. IMPDH2 promotes cell proliferation and epithelial−mesenchymal transition of non-small cell lung cancer by activating the Wnt/β-catenin signaling pathway. *Oncol Lett* 2020;**20**:219.
57. Wu TY, Peng Y, Pelleymounter LL, Moon I, Eckloff BW, Wieben ED, et al. Pharmacogenetics of the mycophenolic acid targets inosine monophosphate dehydrogenases IMPDH1 and IMPDH2: gene sequence variation and functional genomics. *Br J Pharmacol* 2010; **161**:1584−98.
58. Espinar L, Garcia-Cao M, Schmidt A, Kourtis S, Gañez Zapater A, Aranda-Vallejo C, et al. Nuclear IMPDH2 controls the DNA damage response by modulating PARP1 activity. *Nat Commun* 2024; **15**:9515.
59. Kofuji S, Hirayama A, Eberhardt AO, Kawaguchi R, Sugiura Y, Sampetrean O, et al. IMP dehydrogenase-2 drives aberrant nucleolar activity and promotes tumorigenesis in glioblastoma. *Nat Cell Biol* 2019;**21**:1003−14.
60. Quincozes-Santos A, Bobermin LD, Souza DG, Bellaver B, Gonçalves CA, Souza DO. Guanosine protects C6 astroglial cells against azide-induced oxidative damage: a putative role of heme oxygenase 1. *J Neurochem* 2014;**130**:61−74.
61. Dobrachinski F, da Rosa Gerbatin R, Sartori G, Ferreira Marques N, Zemolin AP, Almeida Silva LF, et al. Regulation of mitochondrial function and glutamatergic system are the target of guanosine effect in traumatic brain injury. *J Neurotrauma* 2017;**34**: 1318−28.
62. Souza DG, Bellaver B, Bobermin LD, Souza DO, Quincozes-Santos A. Anti-aging effects of guanosine in glial cells. *Purinergic Signal* 2016;**12**:697−706.
63. Courtes AA, de Carvalho NR, Gonçalves DF, Hartmann DD, da Rosa PC, Dobrachinski F, et al. Guanosine protects against Ca^{2+}-induced mitochondrial dysfunction in rats. *Biomed Pharmacother* 2019;**111**:1438−46.
64. Klaunig JE. Oxidative stress and cancer. *Curr Pharm Des* 2019;**24**: 4771−8.
65. Commoner B, Townsend J, Pake GE. Free radicals in biological materials. *Nature* 1954;**174**:689−91.